Nonlinear Mixing in Optical Multicarrier Systems

By

Mahmood Abdul Hameed

Submitted to the graduate degree program in the Department of Electrical Engineering and Computer Science and the Graduate Faculty of the University of Kansas in partial fulfillment of the requirements for the degree of Doctor of Philosophy.

_____

Chairperson Dr. Rongqing Hui

_____

Dr. Erik Perrins

_____

Dr. Shannon Blunt

_____

Dr. Alessandro Salandrino

_____

Dr. Carey Johnson

Date Defended: Jan. 14th, 2016

The Dissertation Committee for Mahmood Abdul Hameed

certifies that this is the approved version of the following dissertation:

Nonlinear Mixing in Optical Multicarrier Systems

_____

Chairperson Dr. Rongqing Hui

Date approved: Jan. 14th, 2016

Abstract

Although optical fiber has a vast spectral bandwidth, efficient use of this bandwidth is still important in order to meet the ever increased capacity demand of optical networks. In addition to wavelength division multiplexing, it is possible to partition multiple low-rate subcarriers into each high speed wavelength channel. Multicarrier systems not only ensure efficient use of optical and electrical components, but also tolerate transmission impairments. The purpose of this research is to understand the impact of mixing among subcarriers in Radio-Over-Fiber (RoF) and high speed optical transmission systems, and experimentally demonstrate techniques to minimize this impact. We also analyze impact of clipping and quantization on multicarrier signals and compare bandwidth efficiency of two popular multiplexing techniques, namely, orthogonal frequency division multiplexing (OFDM) and Nyquist modulation.

For an OFDM-RoF system, we present a novel technique that minimizes the RF domain signal-signal beat interference (SSBI), relaxes the phase noise limit on the RF carrier, realizes the full potential of optical heterodyne-based RF carrier generation, and increases the performance-to-cost ratio of RoF systems. We demonstrate a RoF network that shares the same RF carrier for both downlink and uplink, avoiding the need of an additional RF oscillator in the customer unit.

For multi-carrier optical transmission, we first experimentally compare performance degradations of coherent optical OFDM and single-carrier Nyquist pulse modulated systems in a nonlinear environment. We then experimentally evaluate SSBI compensation techniques in the presence of semiconductor optical amplifier (SOA) induced nonlinearities for a multicarrier optical system with direct detection. We show that SSBI contamination can be significantly reduced from the data signal when the carrier-to-signal power ratio is sufficiently low.

Acknowledgements

I would like to thank my wife, Aqsa, and my son, Sameer, for being patient and giving me unconditional support over the years. I would also like to thank my advisor, Dr. Rongqing Hui, for his excellent advice, invaluable ideas and suggestions, and encouragement that I have received from him throughout my doctoral program.

Thanks are due to Professors Erik Perrins, Shannon Blunt, Alessandro Salandrino, and Carey Johnson for serving on my dissertation committee and examining my research work.

Table of Contents

Chapter 1

Introduction and Motivation

1.1 Historical Perspective of Optical Communications

The field of fiber-optic telecommunication is rapidly changing with the introduction of new technologies and products to meet the ever increased demand of the information society. Interest in this field can be best gauged by learning about the current research and product development conducted by various companies (Ciena, Corning, JDS Uniphase, Lucent, Alcatel, etc.). It all began in 1970, when researchers at Corning successfully fabricated optical fibers using fused-silica with a loss of less than 20 dB/km at 633 nm wavelength [1]. Over the years, the use of, and demand for, a secure high bandwidth transmission medium such as an optical fiber has grown tremendously. The demand is primarily driven by vast amount of information traffic due to Internet, multimedia, data and video. Laying fiber-optic cable in America started in the 1980s when the systems operated at about 90 Mb/s, with a single fiber capable of handling about 1300 simultaneous channels [2]. At the turn of the last century, this number was over 130,000 simultaneous voice channels with systems operating at 10 Gb/s and beyond. In the last decade or so technologies such as dense wavelength-division multiplexing (DWDM) and erbium-doped fiber amplifiers (EDFA) have further increased data rates to beyond a terabit per second (>1000 Gb/s) over distances in excess of 100 km [3]. This is equivalent to transmitting 13 million simultaneous phone calls through a single hair-size glass fiber.

1.2 Multicarrier Signaling

There are many reasons that make fiber-optic link the perfect choice for transmission. Some of their advantages over twisted pair and coaxial cable include low attenuation, large bandwidth, small diameter and light weight, immunity to electromagnetic interference, security and affordability. Even though the fiber optic medium offers a very large bandwidth (~1 Pb/s [4]), the end user requirement can be much lower (~few hundred Mbps), which is still significantly smaller than the channel capacity of DWDM. With the bandwidth of optical and electrical components in mind, a finer spectral granularity is needed for overall network design to be flexible and efficient. Multicarrier optical systems partition high speed signal into multiple low rate subcarriers. Such division reduces inter-symbol interference and improves tolerance to linear fiber impairments [5-7].

Even though in the optical domain, multicarrier transmission is more advantageous and suitable for future transmission systems compared to a single-carrier system, their comparison in the RF domain is an ongoing debate [8, 9]. Multicarrier optical systems have several strong points in their favor, such as, sub-wavelength bandwidth access for performance monitoring [10], tolerance to linear imperfections, bandwidth scalability [11, 12], allowing higher order modulation [13], and comparable computation complexity [8, 9, 14].

Another important aspect in design of next generation fiber-optic communication systems is spectral efficiency. High spectral efficiency (data rate per hertz of optical bandwidth) is becoming the focus of several research efforts [15-18]. This parameter can be improved in a multicarrier system either by shrinking the spectral bandwidth of each subcarrier (Nyquist-WDM [19]) or by allowing spectral overlap of adjacent subcarriers such as in OFDM [20]. In the case of OFDM, usage of available bandwidth is increased by packing large number of subcarriers.

The presence of multiple subcarriers can make transmission susceptible to inter-subcarrier crosstalk and may set power limitations in certain scenarios. The focus of our research work is to study, theoretically and through experimental results, the performance of, and problems encountered, during multicarrier transmission in various optical system configurations. A brief overview of two popular multicarrier transmission schemes, namely OFDM and Nyquist, is presented in the following subsections.

1.2.1 OFDM overview

Orthogonal frequency division multiplexing (OFDM) is a multicarrier modulation scheme in which data is modulated onto low rate subcarriers such that any two subcarriers are orthogonal to each other. The orthogonality condition requires that these subcarrier sets are placed at frequencies that are spaced at multiples of inverse of the symbol periods [21]. Figure 1.1 shows the frequency domain information (spectrum) of 5 OFDM subcarriers that obey this orthogonality condition. Despite the strong spectral overlap of adjacent subcarriers, subcarrier separation and recovery without inter-subcarrier interference is possible using matched filters as shown by many authors [6, 21, 22]. In time domain, each subcarrier signal is a sequence of rectangular pulses.

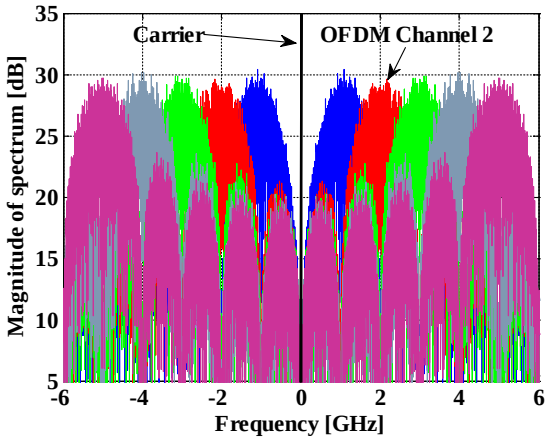

Figure 1.1: Spectrum of 5 OFDM channels; each occupying 2GHz bandwidth.

Partial overlap of subcarriers in frequency allows OFDM to better utilize spectral resources compared to conventional wavelength division multiplexed systems (WDM). Spectral efficiency for OFDM is a direct function of the number of subcarriers. As the number of subcarriers increases, the overall signal spectrum is tightly confined. For these reasons, OFDM based standards are currently being used as digital television standards in Europe, Japan, and most other countries [20, 21], and it is emerging as a promising mode of information transmission for the ever evolving modern optical networks. OFDM, however, has two main problems: (1) high peak-to-average power ratio (PAPR) making it more susceptible to nonlinearities, and (2) sensitivity to frequency and phase noise.

1.2.2 Nyquist overview

OFDM needs the assistance of cyclic prefix (CP) to be able to compensate for chromatic dispersion (CD) [6], thereby reducing the symbol rate. Furthermore, subcarrier separation is possible when orthogonality condition is met, requiring OFDM to have precise subcarrier spacing limits. Hence, recently, Nyquist modulation was proposed that uses sinc-shaped time domain pulses as shown in Figure 1.2 (right) [17, 19, 23, 24], that perform equally well as OFDM with an added advantage of being more flexible. In frequency domain, the sinc-shaped pulses lead to a rectangular spectrum as shown in figure 1.2 (left)

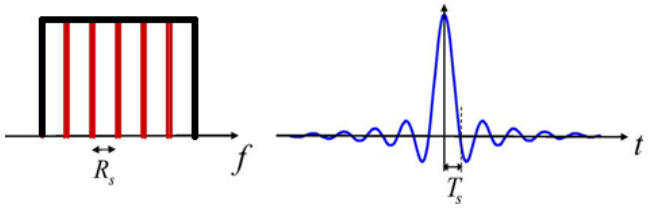

Figure 1.2: Frequency (left) and time (right) domain representation of Nyquist signaling.

Nyquist frequency division multiplexing (NFDM) does not require CP to compensate for CD, nor does it have a limit on subcarrier frequency spacing. Here, the available spectrum is chopped into several (possibly non-equidistant) subcarriers, each modulated with Nyquist pulses. This can be done by simply filtering rectangular pulses with Nyquist filters, described in detail in chapter 4. In contrast with OFDM where subcarrier separation is achieved by integrating over symbol period, in case of Nyquist, sharp rectangular filters select the subcarrier to be recovered.

We have compared OFDM and Nyquist signaling with respect to their bandwidth utilization in chapter 2 and experimentally evaluated and compared their performance in the presence of a nonlinear device in chapter 4. Even though these schemes have differences, they both allow gapless multiplexing to form super channels as shown in Figure 1.3.

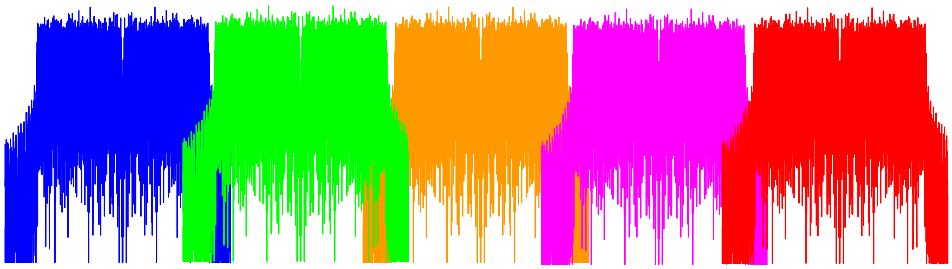

Figure 1.3: Multicarrier modulation allowing gapless multiplexing.

1.3 Detection Methods

In the previous sections, we have established that, unlike the RF domain where there is continuing debate between single-carrier and multicarrier performance, multicarrier transmission certainly has more advantageous, and hence superior, in the optical domain. Performance of an optical system also depends on type of detection used to receive an optical multicarrier signal as the impairments vary depending on whether direct-detection or coherent detection is employed. Signal-to-noise ratio (SNR) in a coherent detection receiver is linearly proportional to input

power of the optical signal, whereas in a direct detection receiver, the SNR is proportional to the square of the input power [1]. Coherent detection has shown to perform significantly better than direct detection when the signal optical power is low. It is to be noted that, full benefit of coherent detection can be achieved when local oscillator (LO) power is much stronger than optical signal power. Coherent detection has great benefits such as better sensitivity and better spectral efficiency but is accompanied with high-cost installations, including narrow linewidth laser sources, local oscillators, 90 optical hybrids, and extra signal processing accounting for the phase and frequency offset estimations.

Even though coherent detection performs better than direct detection in many system aspects, it accounts to costlier and more complicated receivers. On the other hand, direct detection is simple, cheap, and offers practical solutions to optical systems. However, when detecting a multicarrier signal, the square-law operation performed by the photodetector can create second-order modulation products, also termed as signal-signal beat interference (SSBI), which can contaminate the useful data signal. SSBI is not only problematic in optical direct detection receivers, but also in RF domain when down converting a signal to baseband which is required in radio-over-fiber systems (RoF), as will be shown in chapter 3 [25].

1.4 Transmission Impairments

The most basic hurdle in optical transmission is the fiber loss (~0.2 dB/km) that can be overcome by using amplifiers in repeaters with high gain and low noise figure. Single-mode fibers are used for high data rate applications as they are not affected by modal dispersion. However, at high data rates chromatic dispersion (wavelength dependence of fiber's refractive index; different wavelengths travel with slightly different velocities) may be the limiting factor and might lead to pulse spreading. This problem can be overcome by transmitting at 1300 nm range wavelength as

the refractive index is fairly constant or by splicing in a short dispersion-compensating fiber. In long-haul transmission, the noise from amplifiers accumulates thereby reducing the optical signal-to-noise ratio (OSNR). This problem can be solved by increasing the signal power either by reducing the distance between repeaters (increases cost) or by increasing the gain of amplifiers. This leads to a phenomenon known as Kerr effect (refractive index dependence on signal power). Depending upon the type of input signal, the Kerr nonlinearity manifests itself as Self-Phase Modulation (SPM), Cross-Phase Modulation (XPM) and Four-Wave Mixing (FWM). SPM (in single channel system) refers to the nonlinear phenomenon where the changes in refractive index cause phase shift in the time domain pulse, leading to spectral broadening [26]. XPM occurs when two or more wavelengths co-propagate and intensity fluctuations in one wavelength channel causes phase fluctuations in other channels [27]. In wavelength-division multiplexed (WDM) systems, FWM results in power transfer from one channel to the other. New waves are generated at optical frequency $\omega 4$ because of signals at $\omega 1$, $\omega 2$, $\omega 3$ given by $\omega 4 = \omega 1 \pm \omega 2 \pm \omega 3$.

Apart from these, there is another transmission impairment that is specific to multicarrier transmission. SSBI occurs due to subcarriers mixing with each other in the presence of a square-law device. Some of the proposed solutions to this impairment are presented in the following section.

1.5 SSBI Impairment

Several solutions have been proposed to address SSBI in direct detection systems. Lowery et al. have avoided the impact of SSBI on data signal by using band offset modulation (reserving a guard band equal to the signal bandwidth) [6]. This technique however, reduces the spectral efficiency by 50%. Majority of other techniques used to combat SSBI need complex DSP

algorithms to be implemented at the transmitter and/or receiver. Cao et al. have used interleaver and turbo codes to make the triangular SSBI uniform [28]. Peng et al. in [29] use virtual SSB transmission with iterative detection techniques. Li A. et al. have presented experimental demonstration of SSBI noise cancellation using blockwise signal phase switching [30]. SSBI cancellation receivers based on balanced detection (requires additional photodetector) have been demonstrated in [31, 32]. It is to be noted that SSBI is a result of mixing among subcarriers while the desired received signal is obtained due to the mixing between optical carrier and subcarriers. Hence, if the carrier is significantly amplified (at the cost of high carrier-to-signal power ratio and reduced sensitivity), SSBI can be minimized as shown by Schmidt, B.J. et al. [33].

1.6 Summary of Dissertation

The focus of our work is to theoretically and experimentally evaluate the impact of nonlinear mixing in multicarrier signaling in radio-over-fiber (RoF) and direct detection system configurations.

Firstly, in chapter 2, we analyze impact of PAPR, clipping, and quantization on multicarrier signals and later compare electrical bandwidth utilization of two popular multiplexing techniques in orthogonal frequency division multiplexing (OFDM) and Nyquist modulation.

Chapter 3 deals with the proposed solution to SSBI in Radio-Over-Fiber Systems. When a multicarrier signal is used for millimeter wave RoF transmission, SSBI occurs during the RF down conversion process. We proposed and experimentally demonstrated techniques for efficient RF carrier extraction and reuse in an OFDM RoF system. In this system, an RF carrier is generated in the base station through optical heterodyning between two uncorrelated optical carriers delivered from the central office. The RF down conversion is accomplished by mixing the intermediate frequency signal with the extracted RF carrier. This not only relaxes the phase

noise requirement on the RF carrier, but also minimizes signal–signal beat interference. We demonstrate a RoF network carrying 8.2 Gb/s QPSK data in OFDM modulation format for both downlink and uplink, which share the same RF carrier, which avoids the need of an additional RF oscillator in the customer unit. We present our experimental setup and results in detail in Chapter 3 [25].

Chapter 4 deals with the impact of semiconductor optical amplifier (SOA) nonlinearities on fiber-optic systems with coherent detection. We have presented experimental comparison of performance degradations of 20 Gb/s coherent optical OFDM and single carrier Nyquist pulse modulated systems due to the nonlinearity of a SOA [24]. The impact of clipping in the nonlinear region on an OFDM signal is also observed.

In chapter 5, we experimentally evaluate the performance of signal-signal beat interference (SSBI) compensation technique in the presence of SOA-induced nonlinearities for a multicarrier optical system with direct detection.

Lastly in chapter 6, we provide a summary of our research findings work and present possible extensions of this work for modern multicarrier systems.

Chapter 2

System Design Aspects

2.1 Introduction

In this chapter we discuss two important design considerations of multi-carrier systems: (1) the impact of digitizing errors of analog-to-digital converter (ADC)/digital-to-analog converter (DAC) on system performance; and (2) the electrical bandwidth efficiency of OFDM and Nyquist modulated signals.

2.2 Impact of DAC/ADC

Multicarrier signaling schemes such as OFDM and Nyquist-WDM have several advantages of tolerance to chromatic and polarization mode dispersion, and ease of channel and phase estimation, but they suffer from high peak-to-average power ratio (PAPR). Rare high peaks in time domain signal occur when several subcarriers constructively add up within a particular bit time period. A high PAPR can be a significant problem with respect to the digital-to-analog (DAC) and analog-to-digital (ADC) converters employed in the system because of their limited bit resolution. To preserve and efficiently utilize limited resolution of DACs and ADCs, a simple technique such as clipping can be used [21, 34, 35]. Clipping is a way to reduce PAPR by limiting the range of signal amplitude at the cost of rare bit error possibility. In this section, we investigate the impact of bit resolution on performance of the system when clipping, and later quantization, is used. Let *x[n]* and *x'[n]* represent the unclipped and the clipped version of real or imaginary part of a multicarrier signal, respectively. Then *x'[n]* can be written as;

$$x'[n] = \begin{cases} x[n] & -k\sigma \le x[n] \le k\sigma \\ -k\sigma & x[n] < -k\sigma \\ k\sigma & x[n] > k\sigma \end{cases} \qquad (2.1)$$

Where k is the clipping ratio factor and σ is the standard deviation of $x[n]$. Figure 2.1 shows an arbitrary OFDM signal bounded between $-k\sigma$ and $k\sigma$ along with its probability density function (PDF). When the number of subcarriers is large, the PDF tends towards a Gaussian function as per the central limit theorem. Gaussian PDF can be described by its mean (zero mean in this case) and variance, μ (=0) and σ^2, respectively. Hence, the PDF of OFDM signal before clipping can be accurately represented with a Gaussian process as;

$$p(x) = \frac{1}{\sqrt{2\pi\sigma^2}} e^{-\frac{x^2}{2\sigma^2}} \qquad (2.2)$$

Clipping leads to chopping off of some rare high or low peaks, which can be termed as clipping noise. Clipping noise power (σ_{clip}^2) can be computed by integrating the PDF (computing area under the PDF) from clipping boundary to ∞ or $-\infty$.

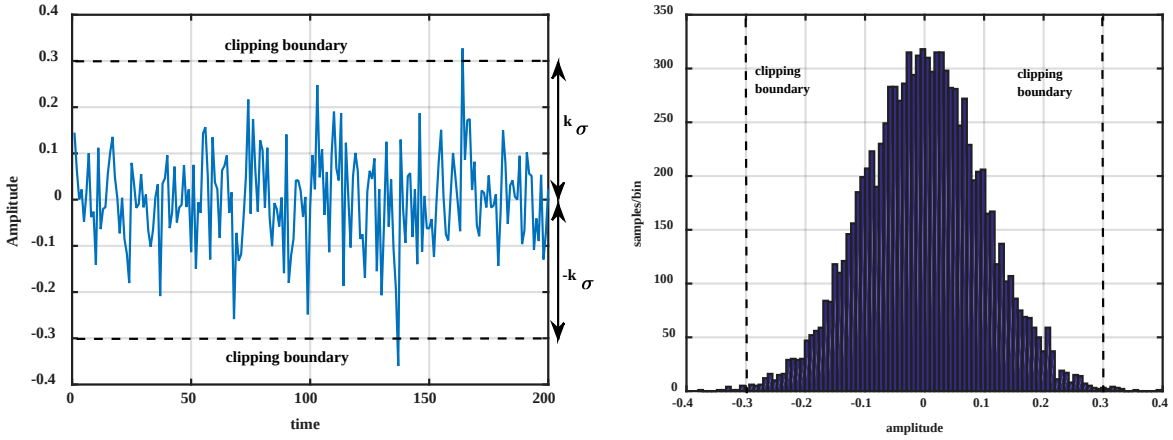

Figure 2.1: Arbitrary time domain OFDM signal (left) and its histogram (right)

$$\sigma_{clip}^2 = 2\int_{k\sigma}^{\infty} (x - k\sigma)^2 \frac{1}{\sqrt{2\pi\sigma^2}} e^{-\frac{x^2}{2\sigma^2}} \mathrm{dx} \approx 2\sqrt{\frac{2}{\pi}} \sigma^2 k^{-3} e^{-k^2/2} \qquad (2.3)$$

The PAPR of a multicarrier signal depends directly on the number of subcarrier signals being multiplexed (PAPR $\propto N$) [36]. As the number of subcarriers increases, the probability of higher

number of subcarriers to constructively add up also increases. We use error vector magnitude (EVM) as our performance metric to evaluate system performance of an OFDM signal with varying number of subcarriers when quantized by a *q*-bit ADC or DAC. EVM is a measure of spreading of the received constellations. A higher EVM signifies poorer performance. Figure 2.2 shows a comparison of EVM performance of an OFDM signal with 10 and 64 subcarriers. It is clear that the performance of 10 subcarriers is overall better than that for 64 subcarriers. This is due to the fact that 64 subcarriers signal has a higher PAPR than that for 10 subcarriers, and hence the quantization error is higher for the 64 subcarriers signal. It is to be noted that generation of OFDM signals for each subcarrier is random in nature and to get an accurate assessment, we average EVM for 100 simulations.

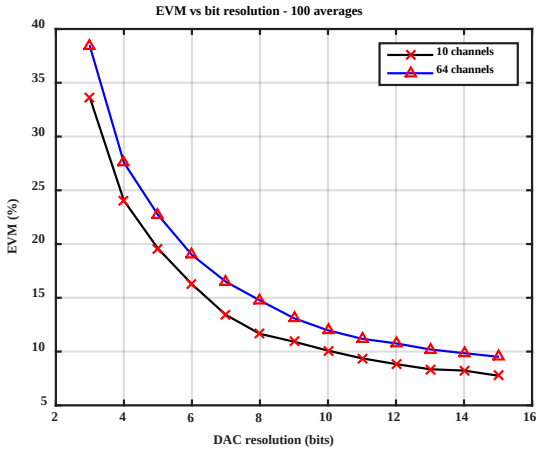

Figure 2.2: Performance comparison of OFDM signal with 10 and 64 subcarriers for varying bit resolution

In a general case, the quantization error for a q-bit resolution ADC/DAC can be written as [37];

$$\sigma_q^2 = \frac{1}{12} \times 2^{-2q} = \frac{(k\sigma)^2 2^{-2q}}{3} \qquad (2.4)$$

When both clipping and quantization errors impact system performance, the signal-to-noise ration can be computed as;

$$SNR = \frac{\sigma^2}{\sigma_{clip}^2 + \sigma_q^2} = \left(2\sqrt{\frac{2}{\pi}} k^{-3} e^{-k^2/2} + \frac{k^2 2^{-2q}}{3} \right)^{-1} \qquad (2.5)$$

Figure 2.3 shows the impact of both clipping and quantization noise on performance of the system measured by SNR. From Figure 2.3 (left), we can clearly see that for each quantization bit resolution, there is an optimal clipping ratio at which the SNR is maximized. For example, the DAC card used in our experiments has the bit resolution of 6-bits. The optimal clipping ratio in our setup based on this analysis would be *k*=3.4.

Clipping and quantization together contribute to a signal processing penalty that can be computed as shown in Equation 2.6;

$$SNR_{penalty} = \frac{10}{\ln(10)} \left(2\sqrt{\frac{2}{\pi}} k^{-3} e^{-k^2/2} + \frac{k^2 2^{-2q}}{3} \right) SNR_{target} \qquad (2.6)$$

Where SNR_{target} is the targeted signal-to-noise ratio to guarantee a certain bit-error-rate (BER). Assuming that required BER is 10^{-3}, the targeted SNR for QPSK modulation format would be about 9.8dB. The SNR penalty is shown in Figure 2.3 (right) for different bit resolutions when clipping ratio is varied.

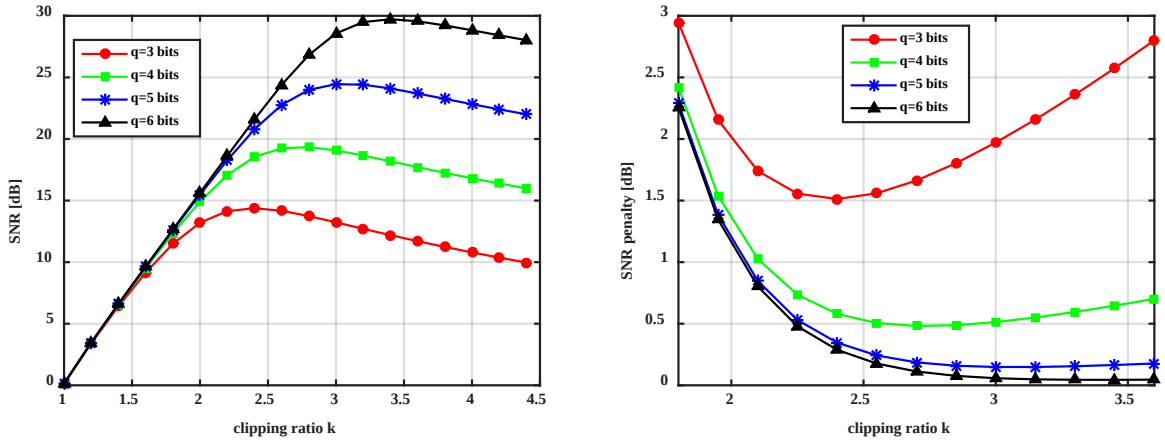

Figure 2.3: SNR (left) and SNR penalty (right) as a function of clipping ratio for different bit resolutions.

From this analysis, we can conclude a few design choices about system setup, bit resolution of DAC and optimal clipping ratios. Figure 2.3 (right) shows that to maintain a SNR penalty under 0.5 dB for a required BER of 10^{-3}, we would at least need 4 bit resolution for the DAC. We also observe that the SNR penalty is severe when 3 or 4 bit DACs are used. As the bit resolution is improved to 5 or 6 bits, the SNR penalty goes down drastically (smaller gap between lines). This means that even if higher bit resolution DACs were available, we would not benefit a whole lot in terms of improving performance. Hence, using a 6-bit DAC in our experiments with QPSK modulation provides a reasonable tradeoff between performance and cost.

2.3 Electrical Bandwidth Utilization of OFDM and Nyquist-FDM

OFDM and Nyquist modulation schemes, as described in previous chapter, have several similarities. They are, in way, simply interchanging time and frequency domain to represent a multi-carrier signal. These two schemes have come to the forefront as multiplexing formats that can deliver record high spectral efficiencies while tolerating linear fiber impairments [17, 24, 36]. With respect to two very critical aspects of system design, i.e. spectral efficiency and PAPR, their performance is almost identical [36]. However, given a certain electrical bandwidth, Nyquist frequency division multiplexing [17] is able to more efficiently utilize the available spectrum, especially for low subcarrier count. This is due to the fact that in OFDM, the spectral efficiency is a function of the number of subcarriers that have to be orthogonal to each other, while for Nyquist spectral efficiency is a function of filter roll-off factor that can be arbitrarily changed. This conclusion is based on the following analysis.

Electrical Bandwidth of OFDM

If the sampling rate of DAC is F_s samples/second being used to quantize an OFDM subcarrier signal, then the electrical bandwidth per subcarrier used would be;

$$\mathrm{BW}_{\mathrm{OFDM}} = \frac{Fs}{Samples\ per\ bit} \qquad (2.7)$$

where *Samples per bit* is an integer greater than 2. Note that, in a multicarrier system, we could have an overall non-integer samples per bit when different subcarriers have different data rates. Here, we are looking at only one subcarrier and hence *samples per bit* has to be an integer.

Electrical Bandwidth of Nyquist

In the case of single carrier Nyquist modulation, the electrical bandwidth is given by;

$$\mathrm{BW}_{\mathrm{Nyquist}} = \frac{1+\beta}{T} \qquad 0 \le \beta \le 1 \qquad (2.8)$$

Where $T = \frac{Samples\ per\ bit}{Fs}$, and β is the filter roll-off factor. *Samples per bit* is an integer greater than 2. Note that, in a multicarrier system, we could have an overall non-integer samples per bit when different subcarriers have different data rates. Here, we are looking at only one subcarrier and hence *samples per bit* has to be an integer. Assuming that *Fs*=20 GSa/s and roll-off factor $\beta = 0$, bandwidth occupied can be plotted against samples per bit, as shown in Figure 2.4 (left).

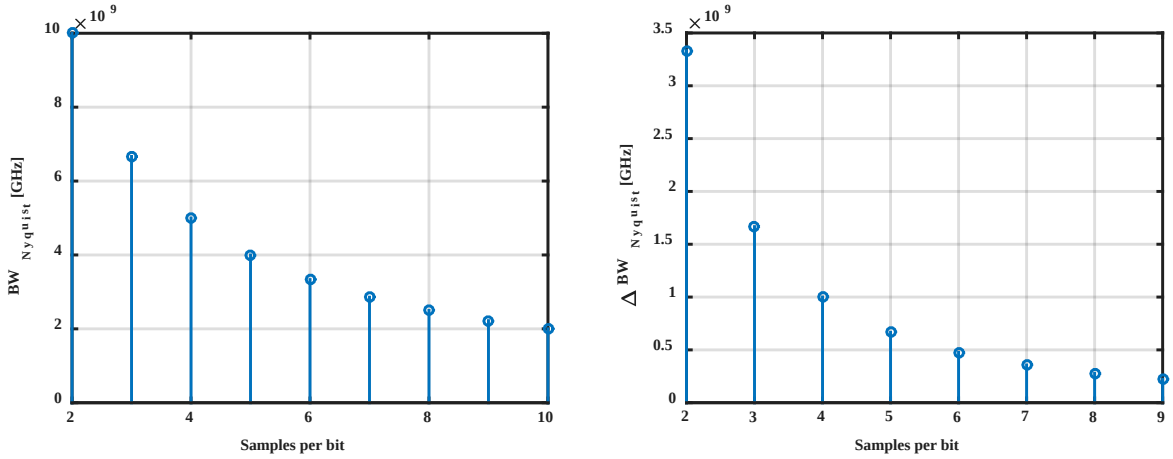

Figure 2.4: Single channel electrical bandwidth utilization as a function of samples per bit (left); differential bandwidth utilization as a function of samples per bit (right)

It can be seen that as the samples per bit increases, the bandwidth occupied by Nyquist goes down in larger steps for lower samples per bit, and smaller steps for higher sample per bit. This means that if available bandwidth is 9 GHz, with OFDM or Nyquist modulation (with $\beta = 0$) we can either use 10 GHz or 6.667 GHz when samples per bit is 2 or 3, respectively. However, when $\beta = 0.12$ and samples per bit =2, Nyquist modulation can achieve a spectral occupancy of 8.98 GHz, improving the granularity of usage of available spectrum. For a given sampling rate and roll-off factor, this granularity becomes finer with increase in samples per bit ($\propto \frac{1}{samples\ per\ bit}$), hence Nyquist-FDM is able to achieve better spectrum utilization for low number of multiplexing channels.

Chapter 3

SSBI in OFDM Radio-Over-Fiber systems

3.1 Motivation

The growing demand of bandwidth for wireless communication networks pushes the RF carrier frequencies to tens of gigahertzes, and toward the millimeter-wave (mm-wave) bands [38]. This enables gigahertz signal bandwidth to be carried on the RF carriers. Millimeter wave frequency bands are more susceptible to atmospheric absorption and rain attenuation compared to lower frequency carriers, and therefore the number of base stations (BS) has to be significantly increased with their locations closer to customer units (CU) to accommodate the reduced transmission distance. In order for such networks to be practical, mm-wave carrier generation in BSs and wideband signal delivering from the central office (CO) to BSs have to be simple and efficient. Radio-over-Fiber (RoF) technology provides a viable solution by delivering mm-wave carriers and high speed data from CO to remote BSs through optical fibers [39]. This allows BSs to be located further away from the CO and minimizes complexity of BSs. At a CU, downstream baseband signal carried on the mm-wave carrier is recovered and digitally processed, and the mm-wave carrier also needs to be regenerated for upstream data transmission.

A number of techniques have been proposed for mm-wave carrier generation and wideband data transport through RoF [39-43].Optical heterodyning is an attractive method which is capable of generating a wide range of carrier frequencies, limited only by the bandwidth of the photodetector. This simplifies the configuration of BSs by optically delivering the mm-wave carrier from the CO to BSs, and therefore most of the complexity is shifted from the BS to the CO. However, the phase noise of the generated millimeter-wave carrier is determined by the

spectral linewidth of the lasers used, which is typically in the tens of megahertz level for a DFB semiconductor laser. Therefore, active phase-locked loop has to be applied to reduce the phase noise of the produced RF carrier [39, 40], and to ensure the quality of the wireless networks carrying phase encoded data. In order to relax the phase noise requirement of the mm-wave carrier, RF self-homodyne has been proposed [41] to down-convert the data signal from IF to the baseband, and therefore conventional DFB laser diodes can be used for optical heterodyne generation of mm-wave carriers without the need of active phase/frequency locking. However, so far, the optical heterodyning technique for mm-wave carrier generation has been used only for the downstream traffic, while the upstream link still requires high-frequency local oscillators for RF carrier generation in BSs and CUs [39, 41, 42, 44, 45]. RF carrier recovery and reuse is therefore highly desirable to realize the full potential of the optical heterodyne technique, and increase the performance-to-cost ratio of RoF systems.

3.2 Principle of operation

In this chapter, we report a technique of RF carrier recovery and reuse in a RoF network based on simple RF filtering. We define Carrier Extraction and Reuse (CER) as a RF technique in which high frequency carrier is extracted using narrowband filtering and reused by mixing it with wide-band data for RF down conversion. Orthogonal frequency division multiplexing (OFDM) is used for data encoding which provides high spectral efficiency and high level of flexibility for spectral shaping [7]. This allows a narrow frequency guard band to be reserved on each side of the carrier, so that it can be selected and recovered by a narrowband RF filter. This extracted RF carrier can then be used to carry the upstream traffic. It is important to note that the multi-subcarrier nature makes OFDM modulation format susceptible to signal-signal beat interference (SSBI) when RF self-homodyne [41] is used for down-conversion from IF to the

baseband. To avoid SSBI, we have modified the RF self-homodyne process by mixing the extracted carrier with the OFDM subcarriers, the technique we refer to as CER.

The difference between RF self-homodyne and CER techniques can be further analyzed by using simple block diagrams as shown in Fig. 3.1 and Fig. 3.2.

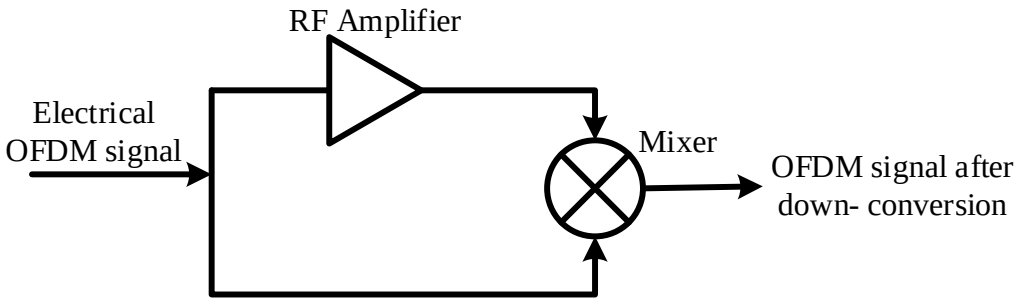

Figure 3.1. Operation of RF self-homodyne technique

In the case of RF self-homodyne technique, the electrical signal after photo detection needs to be down converted to baseband for recovery and demodulation. This is done by mixing the multicarrier with itself as shown in Fig. 3.1. In [41], Islam et al. claim that RF self-homodyne technique is able to avoid phase/frequency locking, but is spectrally inefficient. Simple ASK modulation was used in their experiments that did not have the problem of sub-carriers mixing with themselves, as would happen in a multi-carrier transmission. In order to avoid this situation for a multicarrier case, we attempt to extract the carrier using RF filters and then mix with the wideband multi-carrier signal as shown in Fig. 3.2.

To avoid signal-signal beat interference (SSBI) during down conversion, we use RF filters to extract carrier and an RF amplifier to amply it. We later use this extracted carrier as a local oscillator for down conversion as illustrated in Fig. 3.2. Another benefit of this technique apart of avoiding SSBI, is that the extracted carrier can be used as the uplink carrier.

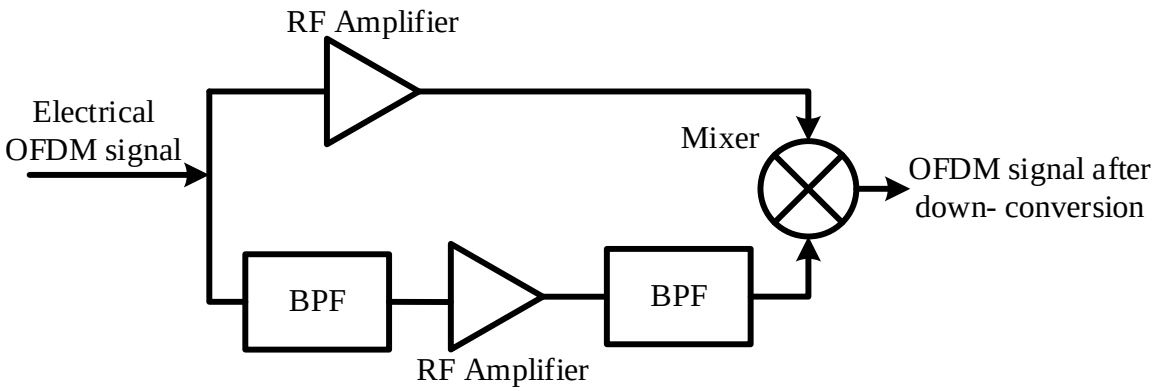

Figure 3.2. Operation of Carrier Extraction and Reuse technique

The performance of these technique in a multi-carrier transmission system can be fairly compared by performing experiments detailed in the following section.

3.3 Experimental Setup

3.3.1 Downlink transmission

Our experimental setup is based on the system as schematically shown in figure 3.3. In the CO, single sideband (SSB) OFDM signal is digitally generated, in which an 8.32 Gb/s serial data is QPSK modulated and loaded onto 48 subcarriers by serial-to-parallel conversion. IFFT operation is performed on a block of length 256. OFDM signal is created by first considering 64 subcarriers and later padding some subcarriers with zeroes to get the desired transmit signal. Each subcarrier occupies rows 1 – 64 while the complex conjugate of the OFDM subcarriers are loaded into rows 193 – 256 in a reverse sequence. This data mapping insures that the time-domain signal has real values after the IFFT operation. Rows 65 – 192 are padded with zeroes to fill up the entire IFFT window. This ensures 2 times oversampling, which takes 4 samples per OFDM period using the 21.418 GSa/s DAC. Hilbert transform is used to generate an electrical SSB OFDM signal after the parallel-to-serial conversion.

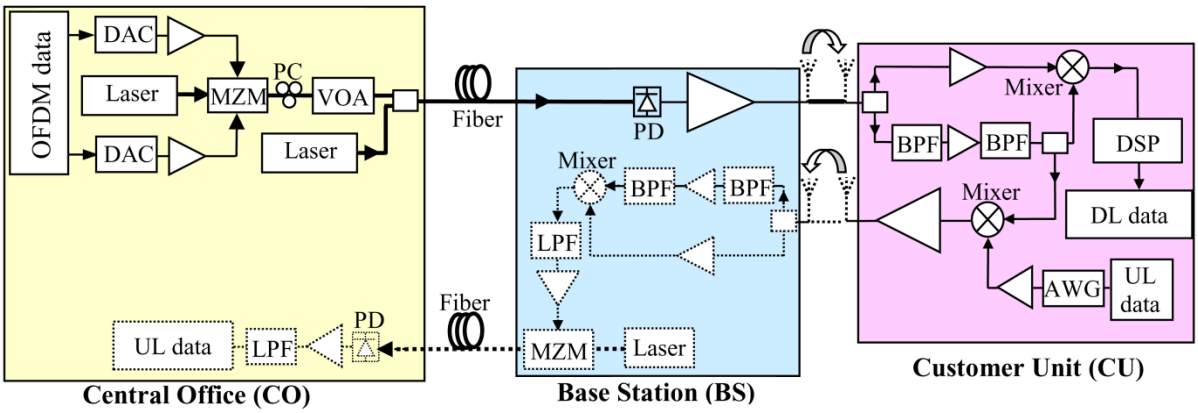

Figure 3.3. Experimental setup for the mm-wave OFDM-RoF system. UL: up-link, DL: down-link, PC: polarization controller, VOA: variable optical attenuator, BPF: band-pass filter, LPF: low-pass filter, AWG: Arbitrary waveform generator, PD: Photo detector, MZM: Mach-Zehnder modulator. Dotted lines indicate functions not been implemented in the experiment but needed for a full duplex system.

A commercial CIENA optical transmitter, which was originally designed for 10 Gb/s SONET systems with electrical-domain pre-compensation (eDCO) [46], is used to generate the optical SSB signal. This card is equipped with two DACs with 21.418 GSa/s sampling speed at 6-bits resolution. It also has a tunable DFB laser (λ_1=1530.720 nm) with approximately 10 MHz spectral linewidth, and a balanced dual-drive MZM. The two arms of the electro-optic modulator are loaded with parallel-to-serial converted IFFT output and the imaginary part of its Hilbert transform respectively. The bias of the dual-drive MZM was set at the quadrature point for optical SSB generation. Another optical carrier from a separate tunable laser at wavelength λ_2=1530.780 nm is combined with the SSB optical signal through an optical coupler before launching into the transmission fiber. Optical heterodyning between the two optical carriers is performed by the photo-detector in the BS which up-converts the OFDM signal onto a high frequency RF carrier at Δf=10.24 GHz (shown in Fig. 3.4 (i)), along with a baseband replica. This RF carrier frequency of 10.24 GHz in our experiment is chosen to demonstrate the system concept because of the availability of RF filters in our laboratory. As Δf is equal to the frequency

difference of the two optical carriers, it can be easily changed to the commercial 60 GHz and 70/80 GHz bands by tuning the optical carriers for mm-wave high data rate applications.

The up-converted RF signal in the BS is then amplified by 30 dB with a wideband (SHF, 30 KHz-40 GHz) amplifier and sent across to the CU. As a proof of concept, an RF cable is used in the experiment in place of the wireless transmission between the BS and CU. Therefore, the impairments of wireless propagation are not included. To recover the data at CU, CER is performed by first splitting the high frequency signal using an RF power splitter (Narda, 2 GHz-18 GHz). At one of the splitter outputs, the RF carrier is selected by a narrowband filters (RLC electronics, 10.24 GHz central frequency, 210 MHz bandwidth) and amplified using an RF amplifier (JCA, 24 dB, 10-20 GHz). The spectrum of the extracted RF carrier is shown in Fig. 3.4 (ii), which provides an RF local oscillator. This local oscillator is mixed with the high frequency signal at the other output of the power splitter using a mixer (Miteq DMX0418L) to down-convert it to the baseband, which is then recorded using a digital oscilloscope with 20 GSa/s sampling rate and 6 GHz bandwidth. Offline Matlab signal processing is used for synchronization, FFT, equalization and demodulating the QPSK downlink data [47].

Even though the bandwidth of the analog-to-digital convertor (ADC) in scope allows us to perform experiments over a 6 GHz spectrum, the intermediate frequency (IF) bandwidth of the available mixer further limits the usable spectrum to 4 GHz. We incorporate this constraint by reducing the number of OFDM subcarriers from 64 to 51, which reduces the actual data rate to 8.7 Gb/s. Moreover, in order for the carrier to be recovered simply by RF filtering, we reserve an approximately 300 MHz guard band by zero-padding the first 3 OFDM subcarriers which are adjacent to the carrier. This further reduces the overall data rate to 8.2 Gb/s.

3.3.2 Uplink transmission

The RF carrier extracted in the CER process and shown in Fig. 3.4(ii) is used to carrier the uplink traffic so that a separate RF oscillator is not required in the CO. The uplink data is a 4 GHz OFDM signal with 3 subcarriers generated by an arbitrary waveform generator (AWG) with 25 GSa/s sampling rate and 10-bit resolution (Tektronix AWG70002A). After mixing with the recovered RF carrier at 10.24 GHz, the uplink RF spectrum transmitted to the BS is shown in Fig. 3.4(iii).

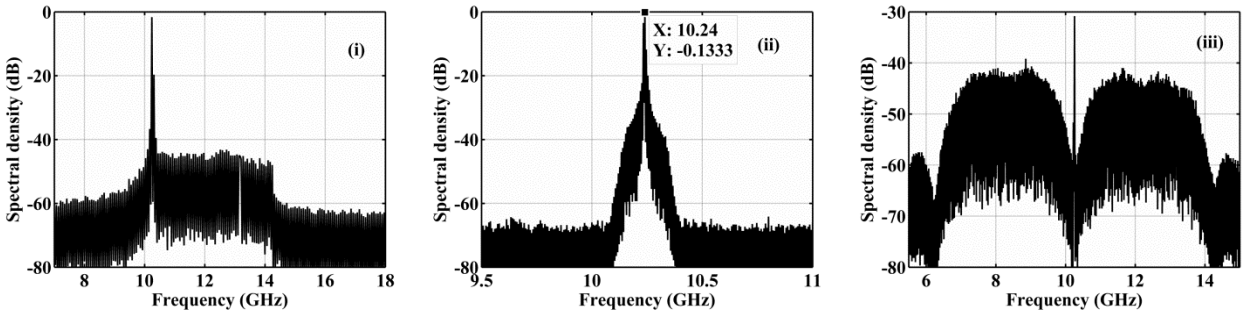

Figure 3.4. RF spectra in downlink and uplink paths, measured after photodetector in BS (i), of the extracted carrier used in CU (ii), and uplink data (iii).

At the BS, CER can again be used which down converts the uplink data to the baseband. This uplink data can then be modulated onto an optical carrier through an electro-optic modulator or using direct modulation on a laser diode if the data rate is low enough. The uplink data is finally recovered in the CO after direct detection and applying similar signal processing routines as in the CU. As the same carrier frequency is used for both the uplink and downlink, time division, or space division multiple access may have to be used to avoid interference in full duplexing [48].

3.4 Results and discussion

In this section, we present the experimental results which compare two techniques of RF frequency down conversion in the downlink path to obtain baseband signal, namely CER and self-homodyne [41]. In self-homodyne, RF signal mixes with itself which is essentially a squaring operation. Whereas in CER, the IF signal mixes with the RF carrier selected by a narrowband filter, which not only provides RF carrier recovery but also avoids SSBI when multi-carrier modulation format is used. We evaluate system performance using Error vector magnitude (EVM) as the performance metric, which is essentially a measure of spreading of received constellation points. EVM has shown to be a reliable metric for high level modulated optical signals including linear and nonlinear impairments [49]. This comparison is performed primarily for the downlink path using OFDM SSB signals with and without a 50% guard-band to show the impact of SSBI. Parameters of the OFDM signals transmitted in these cases are summarized in table 1.

3.4.1. OFDM with 50% guard-band

To observe the effect of nonlinear mixing among subcarriers on the received spectrum, we first consider an OFDM signal that occupies a 2 GHz bandwidth. Fig. 3.5(i) shows the data spectrum digitally generated by a Matlab program which drives the transmitter MZM after DAC and RF amplification. In this spectrum, 2 GHz guard band is reserved on each side of the carrier to elaborate the effect of nonlinear mixing in this region. This is done by forcing the subcarriers 1-27 and 52-64 to zeroes, which is commonly referred to as band offset modulation. Fig. 3.5(ii) and 3.5(iii) show the received baseband spectra at the CU using CER and self-homodyne, respectively, measured with a real-time sampling oscilloscope, and a FFT and frequency equalization process is applied using offline Matlab program.

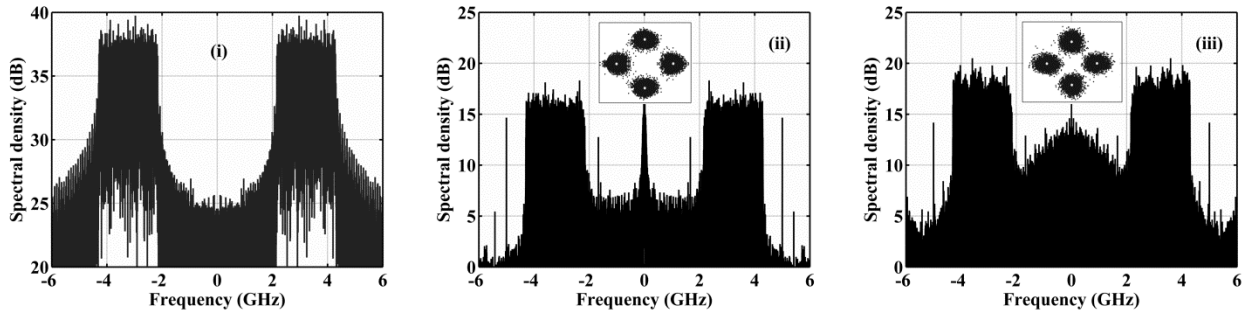

Figure 3.5. OFDM spectra with 50% guard band, generated at the CO (i), measured at the CU using CER (ii) and measured at the CU using self-homodyne (iii). The insets in (ii) and (iii) show the respected received constellation points.

Comparing the two received spectra shown in Fig. 3.5(ii) and 3.5(iii), we see distinct contamination of the spectrum due to SSBI in the 0-2 GHz band when self-homodyne is used. The nonlinear mixing shows a typical triangle shape in the spectrum close to the carrier shown in Fig. 3.5(iii). Here since the 2 GHz guard band is reserved between the carrier and the signal sidebands, the SSBI crosstalk does not affect the receiver performance, and the average EVM of 24 OFDM subcarriers are approximately 15% for both techniques. However, the reduced SSBI in the guard band shown in Fig. 3.5(ii) implies that CER technique does not need this 50% spectral guard band, and thus full bandwidth utilization would be possible for the OFDM signal.

TABLE 3.1: OFDM SIGNAL PARAMETERS

Parameters	50% guard band [units]	w/o 50% guard band [units]	Uplink [units]
	Downlink		
No. of subcarriers	24	48	3
Δf_{sc}	83.66 [MHz]	83.66 [MHz]	1 [GHz]
Unused subcarriers	1-27 and 52-64	1-3 and 52-64	
Data rate	4.18 [Gbps]	8.2 [Gbps]	6 [Gbps]

Δf_{sc} = separation between OFDM subcarriers

3.4.2 OFDM signal with full bandwidth utilization

To measure and compare the impact of SSBI on the received signal with CER and self-homodyne techniques without the 50% spectral guard, we evaluate the EVM for each subcarrier. The transmitted signal in this case occupies the frequency band of 300 MHz - 4.3 GHz consisting of 48 orthogonal subcarriers as shown in Fig. 3.6(i) (generated in Matlab). We reserve a small guard band (0-300 MHz) to isolate the carrier component so that it can be extracted simply with narrowband filtering.

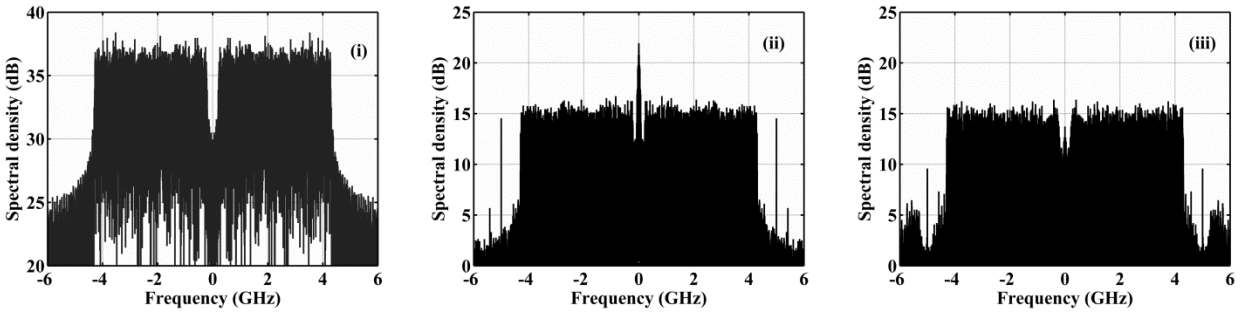

Figure 3.6. OFDM spectra without 50% guard band, generated at the CO (i), measured at the CU using CER (ii) and measured at the CU using self-homodyne (iii).

The corresponding output spectra at the receiver after CER and RF self-homodyne measured using oscilloscope are shown in Fig. 3.6(ii) and 3.6(iii), respectively. Although the shapes of these two spectra look similar, SSBI introduced by nonlinear mixing can be significantly different, especially for the subcarriers adjacent to the carrier.

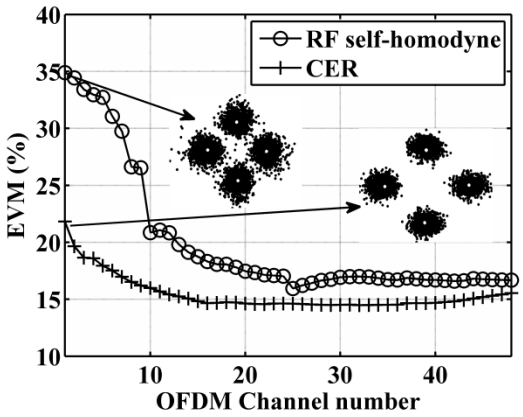

Figure 3.7. Relative system performance for two RF down conversion techniques for each subcarrier. The insets show the received constellations for the first subcarrier for each technique.

Figure 3.7 shows EVM measured as a function of OFDM channel number (1 to 48) for the two RF mixing techniques. It is observed that the performance of CER is substantially better than self-homodyne, for channel numbers lower than 24 indicated by the reduced EVM values. In fact, channels 1 to 24 occupy the 300 MHz to 2.3 GHz region in the spectrum which is expected to be contaminated by triangle-shaped SSBI shown in Fig. 3.5(iii). The EVM of channel 1 (closest to the carrier) for the self-homodyne technique is about 13% higher than that for the same channel when CER is employed. The relative difference in EVM values decreases for subcarriers further away from the carrier. It should be noted that the EVM values from channel 25 to 48 for both techniques were expected to be the same. The small degradation of EVM of self-homodyne at high channel indices is attributed to the slight length imbalance between the two arms leading to the mixer and the introduced phase mismatch before mixing. In addition, for

CER the moderate EVM increase for the first 10 subcarriers near the carrier is due to the phase noise of the RF carrier which is generated by heterodyne mixing between two free-running lasers. As both CER and self-homodyne techniques rely on self-mixing between different components of the heterodyne RF spectrum, their requirements on the frequency stability of the two lasers are expected to be comparable (we show in Appendix A that the phase sensitivity of CER is identical to that of self-homodyne reported for scheme B in [43]), as has been analyzed in [43] for the downlink path. However, further analysis is still needed for the uplink to understand the impact of laser stability using CER.

3.5 Conclusion

We have proposed and experimentally demonstrated a simple carrier recovery and mixing technique where the carrier is generated with optical heterodyning in the BS and extracted with narrowband filtering from the downlink path in the CU. This RF down conversion technique (CER) allows OFDM modulation format to be used but with significantly reduced SSBI compared to RF self-homodyne. Carrier recovery and reuse in the CU makes RoF systems simple and cost effective. The use of multi-carrier modulation enables high bandwidth efficiency and flexibility.

Chapter 4

SOA-Induced Nonlinear Impairments in Coherent Multicarrier Transmission

4.1 Motivation

Semiconductor optical amplifiers (SOA) offer a cost-effective solution for wide-band gain in high data rate fiber-optic systems [50]. Moreover, their small size and ease of integration make them a viable alternative to erbium-doped fiber amplifiers (EDFA) for future optical networks to perform functions such as wavelength conversion, booster and in-line amplification. However, the fast carrier dynamics of an SOA may introduce crosstalk in a wavelength-division multiplexed (WDM) optical system. In recent years, digital processing in optical systems such as coherent optical-orthogonal frequency division multiplexing (CO-OFDM) and single carrier Nyquist pulse modulation (N-PM) systems have been demonstrated to provide record high spectral efficiencies [36], while tolerating linear fiber impairments such as chromatic dispersion (CD) and polarization mode dispersion (PMD) [5-7]. These multiplexing techniques have several other strengths. For example, adaptive rate provisioning is possible in CO-OFDM because it supports digital signal processing at the transmitter and receiver. It also allows bandwidth access at a sub-wavelength granularity [51], self-performance monitoring by precise channel estimation [52, 53], and can lower energy consumption by telecommunication equipment that may have adverse environmental and social impact [54-56]. In an OFDM system, high speed data is partitioned into multiple orthogonal subcarriers each carrying a low data rate, and therefore the overall spectrum is tightly confined within a sharp boundary. On the other hand, N-PM uses high-order Nyquist filters which directly sharpen the edges of the spectrum. Although both of these techniques provide tight spectral confinement to allow gap-less multiplexing for high

spectral efficiency of WDM [19], their susceptibility to system nonlinearity may differ significantly. Our work in this area compares the performance of CO-OFDM and N-PM in a coherent detection nonlinear system where the nonlinearity is introduced by an SOA. Note that, although the nonlinear impact of SOA has been investigated for CO-OFDM and QAM signals [57, 58], the comparison between CO-OFDM and N-PM has not been reported in such a system. Our experimental results indicate that under the same spectral confinement condition, N-PM has better tolerance to SOA nonlinearity compared to CO-OFDM.

4.2 Experimental Setup

The schematic of our experimental setup is shown in Figure 4.1. OFDM and N-PM signals are generated digitally, and the in-phase (*I*) and quadrature (*Q*) components are loaded into the memories of a commercial CIENA optical transmitter which was originally designed for 10 Gb/s SONET systems with the capability of electronic dispersion pre-compensation (*e*DCO) [46].

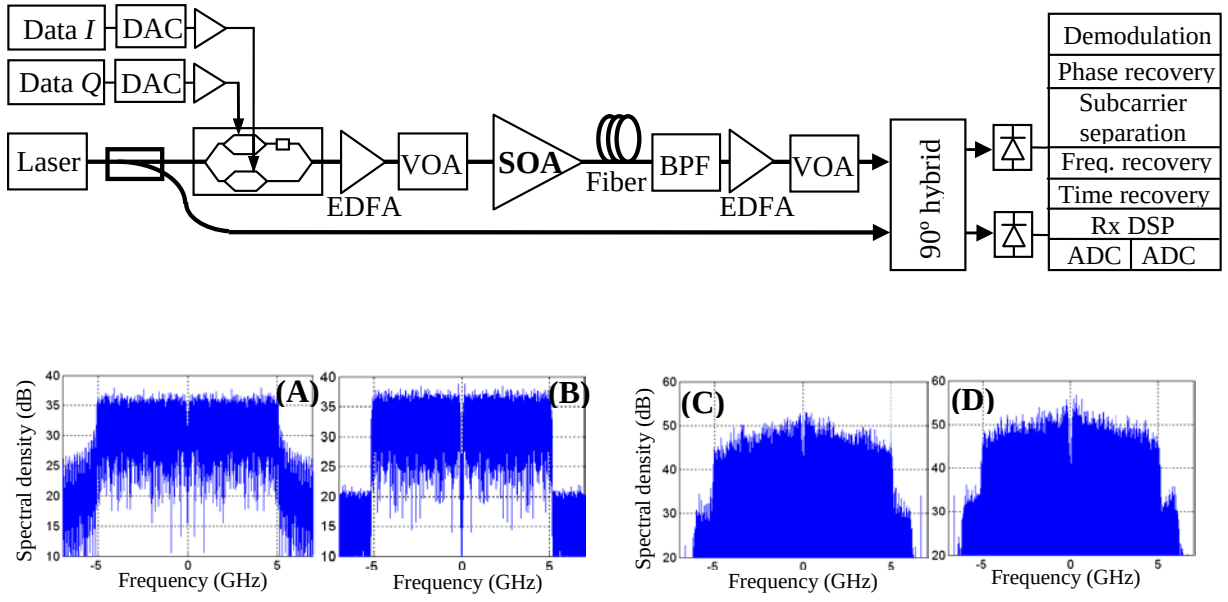

Figure 4.1. Top: Experimental setup, bottom: OFDM (A) and N-PM (B) spectra at the transmitter, and OFDM (C) and N-PM (D) spectra at the receiver. OFDM system has 64 subcarriers and N-PM system has $\beta = 0.03125$.

This transmitter card is equipped with a pair of 22 GSa/s digital to analog convertors (DAC) with 6-bit resolution. The two arms of an electro-optic IQ modulator are driven by the analog waveforms from the DACs through RF amplifiers. A tunable semiconductor laser with 100 kHz linewidth was used both as the light source and as the local oscillator (LO) of coherent homodyne detection.

Both arms of the IQ modulator were biased at minimum transmission point to suppress the optical carrier while the phase shifter is biased at the quadrature point so that the in-phase and the quadrature components of the signal could be mapped onto the upper and the lower optical sidebands. The crosstalk between signals carried by the two sidebands were kept lower than -20dB by carefully adjusting the bias. QPSK data format was used for both OFDM and N-PM systems with the same data rate of 20 Gb/s. While the number of subcarrier channels for the OFDM system varied from 8 to 64 [59], the N-PM system only had a single channel but with different roll off factors β (defined in Equation 4.1) of the Nyquist filter [36], to obtain the comparable spectral roll-off as the OFDM counterpart.

$$H_{TX}(f) = \begin{cases} \frac{\pi f t}{\sin(\pi f t)} & |f| \le \frac{1-\beta}{2T};\ 0 \le \beta \le 1 \\ \frac{\pi f t}{\sin(\pi f t)} \cos\left\{\frac{\pi T}{2\beta}\left(|f| - \frac{1-\beta}{2T}\right)\right\} & \frac{1-\beta}{2T} \le |f| \le \frac{1+\beta}{2T} \\ 0 & |f| \ge \frac{1+\beta}{2T} \end{cases} \quad H_{RX}(f) = \begin{cases} 1 & |f| \le \frac{1-\beta}{2T};\ 0 \le \beta \le 1 \\ \cos\left\{\frac{\pi T}{2\beta}\left(|f| - \frac{1-\beta}{2T}\right)\right\} & \frac{1-\beta}{2T} \le |f| \le \frac{1+\beta}{2T} \\ 0 & |f| \ge \frac{1+\beta}{2T} \end{cases} \tag{4.1}$$

The Nyquist transmit filter described in equation 4.1 is used for pulse shaping and limiting the signal bandwidth. On the other hand, the receive filter is used for channel selection and noise reduction. Figure 4.2 shows the filter transfer functions for varying values of filter roll-off β.

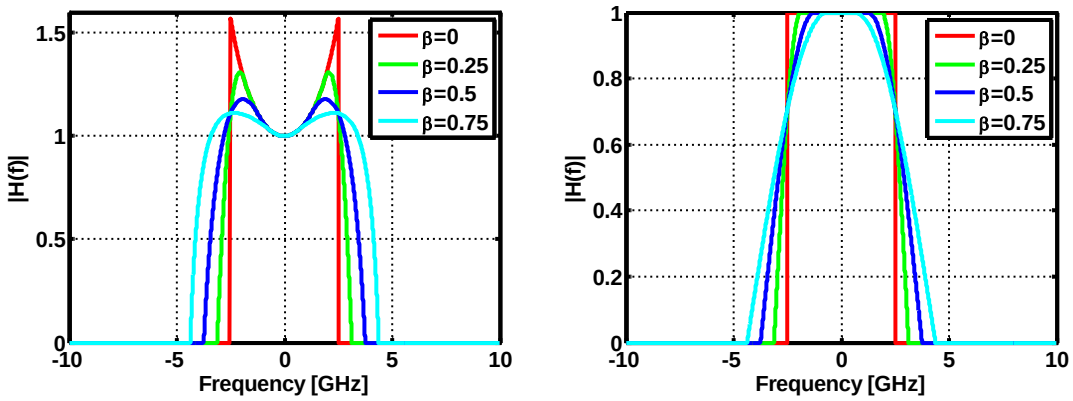

Figure 4.2: Nyquist filter transfer functions for T=0.2 ns with varying values of roll off factor β; transmit filter (left) and receive filter (right)

In the case of OFDM, Digital Subcarrier Multiplexing (DSCM) format is used to digitally generate subcarrier channels and linearly up-convert to an optical carrier using an IQ modulator. Such multiplexing technique benefits from flexible bandwidth allocation and scalability in data rate granularity without compromising the high bandwidth efficiency. To provide flexible bandwidth allocation the spectrum-sliced elastic optical path network (SLICE) [60] has been previously studied, where bandwidth is allocated to a particular service based on the demand for that service by "slicing off" spectrum resources. In such a system, optical carriers are generated using a comb generator, individually modulated by independent data sources, and recombined before transmission. Experimentally, 10 Gb/s, 40 Gb/s, and 100 Gb/s data rates per optical carrier have been demonstrated. Even though such a configuration is able to achieve data rates up to terabits per second, it is not granular enough from a network point of view. Frequency combs with very small channel spacing and the use of many electro-optic modulators is inefficient and unrealistic. Data rate granularity can be improved significantly by generating all subcarriers digitally in the electrical domain and subcarrier allocation can be controlled digitally. We refer to

such format as DSCM. The benefits of DSCM format include simple transmitter implementation and the ability to use digital signal processing techniques for better reliability and flexibility.

An EDFA post amplifier was used at the transmitter output to provide enough optical power to investigate the nonlinear effect of the system, and a variable attenuator was used to adjust optical power launched into the SOA. We used an INPHENIX IPSAD 1501 SOA at 200 mA bias current. The SOA has a small signal gain of 15.4 dB and saturation power of -9.2 dBm. The simulated and measured gains versus input signal power are plotted in Fig. 4.3.

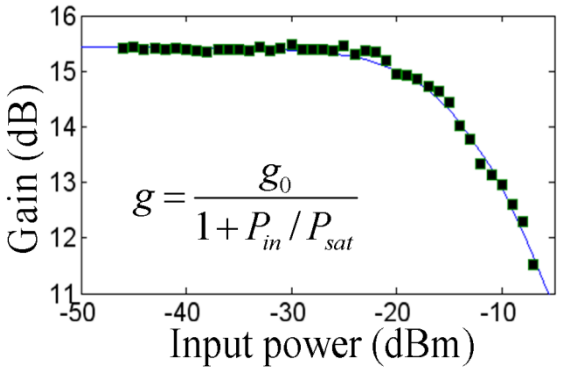

Figure 4.3. SOA nonlinear transfer function. Blue line plot is the simulated gain and the squares are the corresponding experimentally measured values for SOA gain.

Fig. 4.4 shows through simulation, the impact of gain saturation effect (captured in Fig. 4.3) on an arbitrary time domain signal. It is observed that when the instantaneous power of input signal gets close to or beyond the input saturation power of SOA, the time dependent gain goes down thereby clipping the peaks at the output of SOA.

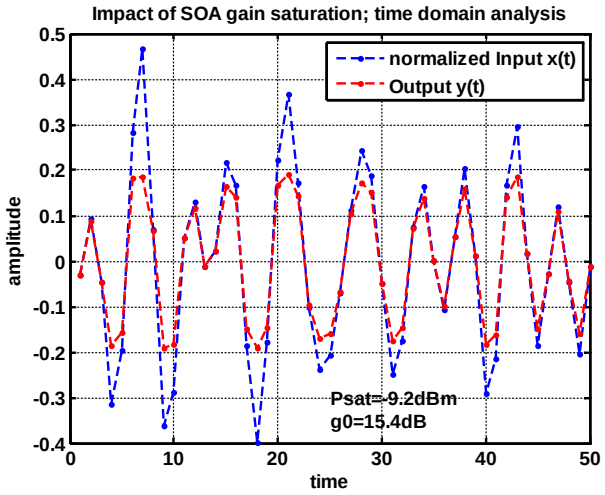

Figure 4.4: Time domain analysis of impact of SOA gain saturation

After an optical band pass filter (BPF) to remove wideband ASE noise, a variable attenuator was used to regulate the received power. The same laser was used for the transmitter and the LO for coherent detection. The LO was combined with the signal in a 90 degree optical hybrid. In-phase and quadrature components of the signal were recovered using separate photo detectors and the electrical signals were recorded using a 20 GSa/s, 6 GHz analog bandwidth, real-time digital scope. Offline signal processing performs time and frequency synchronization, as well as phase recovery using a 4^{th} power Viterbi-Viterbi phase estimation algorithm [59]. OFDM subcarrier separation was performed by digital integration with an FIR filter, while a Nyquist receiving filter was used for N-PM [36].

4.3 Results and discussion

We use Error vector magnitude (EVM) as the performance metric for comparison. EVM has shown to be a reliable metric for high level modulated optical signals including linear and nonlinear impairments [49].

$$EVM \approx \left[\frac{1}{OSNR} - \sqrt{\frac{32}{\pi \times OSNR}}\frac{e^{-0.5\times OSNR}}{2} + 2erfc\left(\sqrt{0.5 \times OSNR}\right)\right]^{0.5} \quad (4.2)$$

4.3.1 Input power influence

Fig. 4.5 shows the EVM measured as a function of input power P_{in} injected into the SOA, where P_{in} was adjusted by varying the attenuation of the VOA. Since the power at the receiver is held constant, P_{in} change is associated with the change in optical signal-to-noise ratio (OSNR) which is shown as the upper axes in Fig. 4.5. The OSNR values were measured by an optical spectrum analyzer (OSA) with 0.1 nm spectral resolution.

For the OFDM system, the number of digitally multiplexed subcarriers varied from 8 to 64 while the total data rate was fixed as 20 Gb/s, and EVMs shown in Fig. 4.5 (A) were averaged over all subcarrier channels. In the linear operation regime with P_{in} <−25dBm, EVM decreases with the increase of P_{in} due to the increase of OSNR. However, system degradation due to SOA nonlinearity takes over for P_{in} >−20dBm where further increase of P_{in} results in the enlarged EVM. Although EVM in the linear operation regime is independent of the number of subcarriers, the EVM degradation due to SOA nonlinearity increases with the number of subcarriers. This is attributed primarily to the effect of four-wave mixing (FWM) among subcarriers. EVM as the function of OSNR in an ideal system can be calculated based on Equation 4.2 [49], which is also shown in Fig. 4.5 for comparison. The floor of measured EVM at 15% is due to the lack of clock

phase synchronization between DACs in transmitter card and the ADC in the digital scope. We have applied clipping to reduce the peak-to-average power ratio (PAPR) of multi-carrier OFDM waveform, although it slightly improved the EVM due to the reduced digitizing error for small signals, the same impact was observed in the linear and nonlinear regimes.

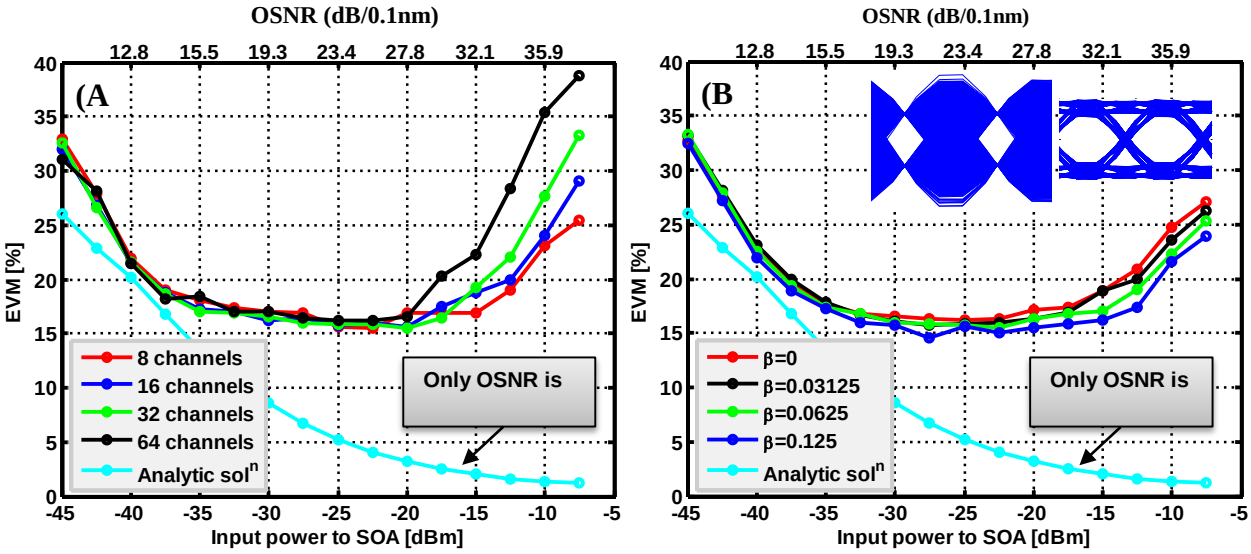

Figure 4.5: EVM measured as a function of input power launched into SOA. (A): OFDM system for varying number of subcarriers, and (B): single-carrier N-PM system with different roll-off factor β. Inset in (B): Transmit eye-diagrams for β =0 (left) and β =0.5 (right)

Fig. 4.5(B) shows the measured EVM values of N-PM system with different roll-off factors of the Nyquist filter. Although EVM versus OSNR characteristics are similar for N-PM and OFDM in the linear regime, the EVM degradation due to SOA nonlinearity in N-PM system is significantly less compared to that in OFDM. Fig. 4.5(B) also indicates the increased EVM degradation in nonlinear regime with reducing the roll-off factor of the Nyquist filter. This is attributed to the decreased time jitter tolerance of eye opening with small roll-off factor as illustrated in insets of Fig. 4.5(B). The spectral confinement of N-PM signal can be improved by decreasing the Nyquist filter roll-off factor β, while the spectral confinement of an OFDM signal

depends on the number of subcarriers. For example, the actual spectral roll-off in a 64 subcarrier OFDM system is equivalent to β = 0.03125 for an N-PM system as indicated in Fig. 4.1 which illustrates the spectra of digitally composed OFDM and N-PM signals at the transmitter and the corresponding spectra at the receiver. The lines of same color in Fig. 4.5(A) and 4.5(B) represent EVMs of OFDM and N-PM systems with the same spectral confinement. While OFDM system suffers from severe crosstalk due to FWM among subcarriers, N-PM system is primarily affected by self-phase modulation (SPM) in the nonlinear regime. We have also observed that phase error dominates in the nonlinear regime for both multiplexing schemes.

4.3.2 Clipping in Nonlinear region

One of the main drawbacks of a multi-carrier transmission scheme such as OFDM is the high peak-to-average power ratio (PAPR). A high PAPR leads to degradation in performance due to nonlinearity in a transmission fiber or SOA for a relatively high launch power. In addition, there are other nonlinear system components namely, Mach-Zehnder modulator (MZM) and DAC/ADC that also introduce distortion.

PAPR depends directly on the number of subcarriers being multiplexed for efficient use of available bandwidth. Spectral efficiency of OFDM signals (Equation 4.3) can be increased by increasing the number of subcarriers.

$$\mathrm{SE_{OFDM}} = \frac{\log_2 M}{1 + \frac{1}{N}} \qquad (4.3)$$

Where $M = 2^{bits/symbol}$ for the subcarrier modulation scheme and N is the number of subcarriers. This means, even though increasing subcarriers is desirable to improve spectral efficiency, it adversely degrades nonlinear performance of the system. One of the simplest ways

to reduce PAPR is clipping [61, 62], in which the peaks of OFDM signal are cut off. Note that excessive clipping can cause bit errors. We define clipping ratio as;

$$\text{Clipping ratio} = \frac{\text{pk-pk amplitude of clipped signal}}{\text{pk-pk amplitude of original signal}} \qquad (4.4)$$

Fig. 4.6 (A) shows an inverse relation between clipping ratio and PAPR. We observe through Monte Carlo simulations that as the clipping ratio is increased (signal is clipped more), the range of PAPR decreases.

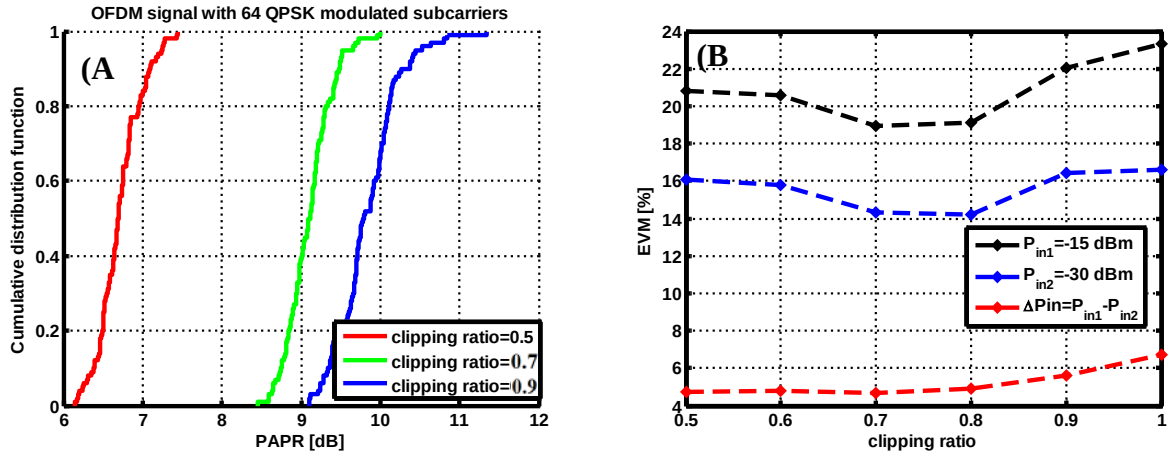

Figure 4.6: Impact of clipping on an OFDM signal with 64 subcarriers. (A): CDF of PAPR for various clipping ratios. (B): Performance of clipped signals in linear and nonlinear regions.

Fig. 4.6 (B) shows the EVM performance of OFDM signals that have been clipped for various clipping ratios ranging from 0.5 to 1 in linear (P_{in}=−30dBm) and nonlinear (P_{in}=−15dBm) regions. We notice that as we begin to clip the OFDM signal, there is an improvement in performance for both linear and nonlinear regions due to the reduction in PAPR. However, further clipping (clipping ratio below 0.7) leads to degradation. The differential of the two line plots in Fig. 4.6 (B) gives us an interesting result. It is observed that nonlinear region in fact benefits more from clipping than linear region.

4.4 Conclusion

We have experimentally compared the performance degradation of CO-OFDM and N-PM schemes due to the nonlinearity introduced from an SOA. It was observed that Nyquist sinc-pulse transmission suffers less nonlinear degradation compared to CO-OFDM at the same spectral confinement condition. More specifically, in a CO-OFDM system nonlinear degradation increases significantly with the increase of the number of subcarriers, while in an N-PM system nonlinear degradation only increases slightly with the decrease of roll-off factor β.

Chapter 5

SSBI Compensation in Multicarrier Optical Systems with Direct Detection

5.1 Motivation

Digital signal processing in recent years has allowed electronic domain compensation of linear fiber impairments such as chromatic dispersion and polarization mode dispersion in multi-carrier optical transmission systems [5-7]. Orthogonal frequency division multiplexing (OFDM) is a multicarrier signaling format that can provide high degree of flexibility and high spectral efficiency. In OFDM, high speed data is partitioned into multiple orthogonal subcarrier channels, and therefore the overall spectrum is tightly confined within a sharp boundary [36]. Direct-detection optical OFDM (DD-OOFDM) provides a low-cost alternative to coherent-detection as it does not require the optical local oscillator in the receiver and the associated complication of wavelength and optical phase tracking. DD-OOFDM usually suffers from signal-signal beat interference (SSBI) originated from nonlinear mixing among signal subcarriers in the photodiode which performs square-law detection. This nonlinear crosstalk may significantly degrade the performance of DD-OOFDM, especially of the low frequency subcarrier channels [63]. Band-offset modulation, also called as offset OFDM, [6] has been used to eliminate SSBI in DD-OOFDM, but it sacrifices 50% bandwidth efficiency. The impact of SSBI can also be reduced by increasing the carrier-to-signal power ratio (CSPR) [33], but this is associated with the degradation of receiver sensitivity.

Iterative SSBI compensation in the digital domain has been demonstrated [29], which preserves the bandwidth efficiency and the receiver sensitivity. While this technique has been shown effective in an optical system operating in the linear regime, its effectiveness in the nonlinear

regime has not been investigated. We have used a semiconductor optical amplifier (SOA) in the system as a controlled nonlinear medium to investigate the impact of nonlinear transfer function in SSBI compensation. Our experimental results show that the nonlinear transfer function in the optical system makes the digital SSBI compensation less effective, especially at high levels of carrier-to-signal power ratio. In addition to providing a nonlinear transfer function for the investigation of system performance, SOA, as a small-size and integrable device, may also offer a cost-effective solution in optical transmitters for applications in metro optical networks [24, 57].

Based on how the multicarrier OFDM signal is generated, direct detection OFDM is classified either as linearly mapped or nonlinearly mapped direct detection OFDM.

5.2 Linearly Mapped Direct Detection OFDM

In the case of linearly mapped DD-OOFDM, the optical OFDM signal is a replica of the electrical baseband OFDM signal and also includes an optical carrier. The optical carrier power is usually the same as the optical signal power. The placement of the carrier with respect to the signal can either be in the offset modulation format [6] (carrier is one OFDM spectrum bandwidth away from the signal) or it can be inserted at the edge of the OFDM signal spectrum as is done in virtual single sideband OFDM (VSSB-OFDM) [64]. Mathematically, this linearly mapped DD-OOFDM can be represented as;

$$s(t) = e^{j2\pi f_0 t} + s_B(t) \cdot \alpha e^{j2\pi (f_0 + \Delta f)t} \qquad (5.1)$$

Where *s(t)* is the optical OFDM signal, f_0 is the optical carrier frequency, Δf is the guard band between carrier and signal, and α is the scaling factor that can be used to adjust the relative

power between the carrier and multicarrier signal. $s_B(t)$ is the baseband OFDM signal described in Equation 5.2.

$$s_B(t) = \sum_{k=\frac{-N}{2}+1}^{\frac{N}{2}} X_k e^{j2\pi f_k t} \qquad (5.2)$$

Where X_k is the OFDM symbol, N is the total number of OFDM subcarriers, and f_k is the frequency of the k[th] OFDM subcarrier. When the optical signal passes through fiber cable, it accumulates chromatic dispersion (CD) and can be approximated as;

$$r(t) = e^{(j2\pi f_0 t - \emptyset_D(-\Delta f) + \varphi(t))} + \alpha e^{j(2\pi(f_0+\Delta f)t + \varphi(t))} \cdot \sum_{k=\frac{-N}{2}+1}^{\frac{N}{2}} X_k e^{\left(j2\pi f_k t + \emptyset_D(f_k)\right)} \qquad (5.3)$$

$$\emptyset_D(f_k) = \pi \cdot c \cdot D_t \cdot {f_k^2}/{f_0^2} \qquad (5.4)$$

Where $\emptyset_D(f_k)$ is the phase delay due to CD for the k[th] subcarrier, D_t is the accumulated CD, and c is the speed of light. The photodetector performs a square law detection and the resulting photocurrent can be written as;

$$\begin{aligned} I(t) \propto |r(t)|^2 &= \eta |r(t)|^2 \\ &= 1 + 2\alpha Re\left\{ e^{j2\pi\Delta f t} \sum_{k=\frac{-N}{2}+1}^{\frac{N}{2}} X_k e^{\left(j2\pi f_k t + \emptyset_D(f_k) - \emptyset_D(-\Delta f)\right)} \right\} \\ &\quad + |\alpha^2| \sum_{k_1=-\frac{N}{2}+1}^{\frac{N}{2}} \sum_{k_2=\frac{-N}{2}+1}^{\frac{N}{2}} X_{k_2}^* X_{k_1} e^{\left(j2\pi(f_{k_1}-f_{k_2})t + \emptyset_D(f_{k_1}) - \emptyset_D(f_{k_2})\right)} \end{aligned} \qquad (5.5)$$

Where η is the responsivity of the photodetector. In equation 5.5, the first term is a DC component that can be easily filtered out. The second term is the useful fundamental term

consisting OFDM subcarrier information that needs to be received. The third term is the second-order intermodulation term referred to as SSBI that needs to be removed from the received signal. The techniques to minimize SSBI, principles, their advantages and disadvantages are discussed in the next section.

5.2.1 Techniques to minimize SSBI

Offset SSB-OFDM: A guard band that is equal to the OFDM spectrum bandwidth is allocated between optical carrier and optical OFDM signal such that the second and third terms of equation 5.5 don't overlap in frequency. This was, the intermodulation term, or SSBI can be removed using a RF filter. To illustrate the effect of SSBI nonlinear mixing among subcarriers on the received spectrum in such a setup, we first consider an OFDM signal that occupies a certain bandwidth (say 2.5GHz) equal to the guard band between carrier and signal as shown in Fig. 5.1(A).

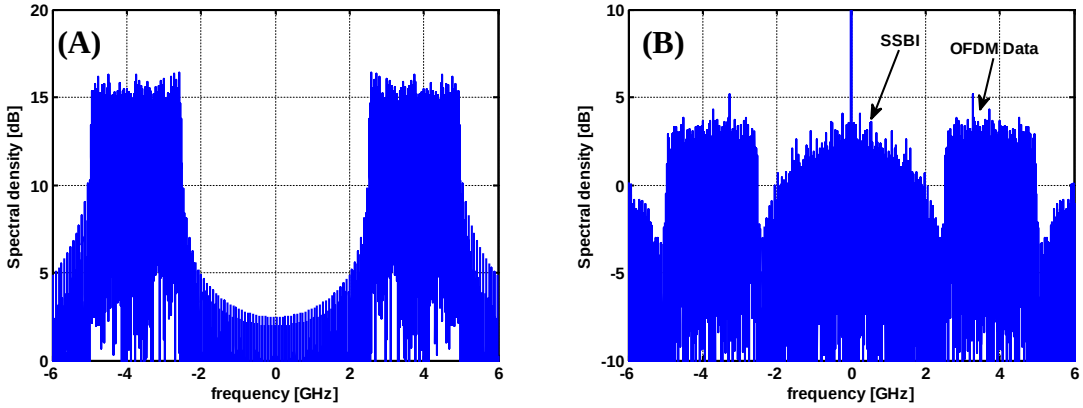

Fig. 5.1: Illustration of SSBI (simulation) in Offset-SSB modulation. (A): Transmit OFDM signal with 32 subcarriers. (B): Direct detection received signal with SSBI present between carrier and data signal.

Fig. 5.1(A) shows the data spectrum digitally generated by a Matlab program which drives the transmitter MZM after DAC and RF amplification. In this spectrum, 2.5 GHz guard band would be reserved on each side of the carrier to elaborate the effect of nonlinear mixing in this region.

Fig. 5.1(B) shows the simulated spectrum of the received signal when direct detection is performed. Due to the square law operation at the photodetector, we see that inter-subcarrier mixing renders the spectrum between carrier and data signal useless, effectively reducing the system bandwidth by 50%.

Baseband optical SSB-OFDM: In this technique the optical carrier is much stronger than the OFDM signal. The scaling factor α is reduced to a very low value in order for the third term to become insignificant. Even though this approach has the advantage of better spectral efficiency, it suffers tremendously because of its poor receiver sensitivity [7, 65].

RF tone assisted OFDM: The two techniques previously mentioned either are spectrally inefficient (Offset-SSB) or have poor receiver sensitivity (Baseband SSB-OFDM). To solve these issues, Peng et al. proposed RF tone assisted OFDM in [66]. Two variations of such technique have been demonstrated. The first variant is similar to Offset-SSB with a slight modification of using an RF tone instead of optical carrier for detection. The second variant has OFDM data on odd orthogonal subcarriers and the even subcarriers are cero padded. The principles of these two variants are shown in Fig. 5.2. The optical carrier in both these cases is suppressed by biasing both arms of an IQ modulator at the minimum point and an RF tone that is inserted at the left edge of electrical spectrum is used for direct detection.

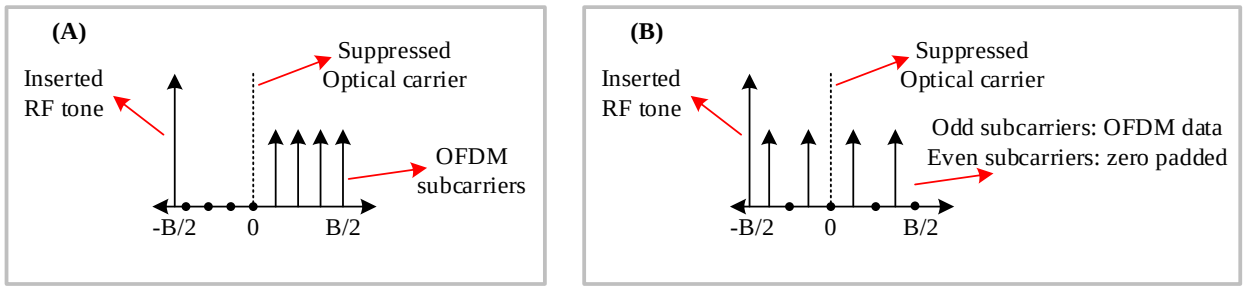

Figure 5.2: Two variants of RF tones assisted OFDM, (A): First variant similar to Offset-SSB. (B): Second variant with OFDM data on odd subcarriers and even carriers filled with zeros.

It is to be noted that such OFDM data configurations results in complex valued signal whose real part and imaginary part are used to drive the two arms of the IQ modulator. For single sideband transmission, the phase shifter is biased at the quadrature point. When the optically modulated signal is detected using a photodetector, the resulting spectra for the above two variants is shown in Fig. 5.3.

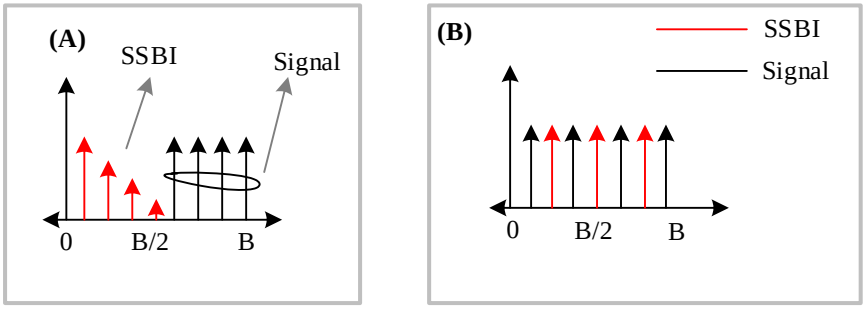

Figure 5.3: Spectrum of detected signal for two variants of RF tones assisted OFDM, (A): First variant with SSBI between 0 and B/2. (B): Second variant with alternating SSBI and OFDM signal.

Thus the interference from second order intermodulation term in both these variants does not distort the OFDM subcarriers.

Virtual SSB-OFDM (VSSB-OFDM): Previously discussed Offset-SSB and RF tone assisted OFDM techniques suffer from inefficient utilization of available system bandwidth. To improve receiver sensitivity and spectral efficiency, Peng et al demonstrated VSSB-OFDM [64]. The optical carrier is again suppressed and not used for detection. Instead a RF tone is inserted at the leftmost OFDM subcarrier, which after optical modulation acts the optical carrier for detection purpose. The two arms of the IQ modulator are driven by the real and imaginary values of the complex valued OFDM signal, whose subcarrier arrangement is shown in Fig. 5.4(A). The main optical carrier from the optical source is suppressed by biasing each arm of modulator at minimum point while the phase shifter is biased at quadrature point for SSB transmission.

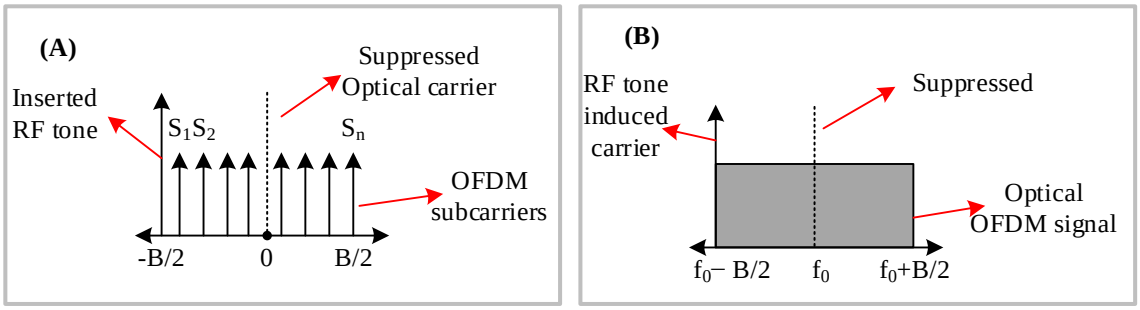

Figure 5.4: Electrical and optical spectra for VSSB-technique, (A): Spectral arrangement of OFDM subcarriers in the electrical signal. (B): Optical signal at the output of IQ modulator with suppressed main optical carrier.

In such transmission configuration, the carrier-to-signal power ratio (CSPR) plays a critical role in terms of the end-to-end performance. CSPR is defined as the ratio of the power in the RF induced optical carrier to the total OFDM optical signal power. Obviously, when the CSPR is high, SSBI would be small as third term in Equation 5.5 would be relatively much smaller than the useful second term. This is similar to the Baseband SSB-OFDM approach proposed by Hewitt [65]. For a low CSPR, SSBI interference is significant and Peng et al. propose a iterative cancellation technique to remove this intermodulation nonlinearity.

There are clear pros and cons of each technique mentioned in this section. For example, Baseband SSB-OFDM has better spectral efficiency, but suffers from low receiver sensitivity. Additionally, VSSB-OFDM technique demonstrates good spectral utilization and has high receiver sensitivity at the cost computational complexity. We focus on VSSB-OFDM approach for our work as there has been tremendous progress in electronic digital signal processing (DSP) for optical communication in the last two decades. Powerful silicon chips with filters and large number of taps, high speed digital-to-analog convertors (DAC), and high speed electro-optic

modulators have made the optical community put more complexity burden on DSP modules and thereby being able to independently optimize the use of each available resource.

5.3 Nonlinearly Mapped Direct Detection OFDM

Nonlinearly mapped DD-OFDM is the second category of DD-OFDM in which the optical signal is no longer the linear translation of the electrical OFDM signal. Here linear mapping takes place between the electrical baseband OFDM signal and the optical intensity. One such mapping is proposed by Schuster et al. [67] called Compatible-SSB OFDM (C-SSB) that can achieve higher spectral efficiency than Offset-SSB modulation. The main advantage of using C-SSB is to reduce the SSBI in direct detection systems. This phenomenon can be easily demonstrated mathematically. An OFDM optical field can be expressed by a summation of the optical carrier and multiple OFDM signal subcarriers as [68],

$$\tilde{x}(t) = A_0 \left[1 + \sum_{k=0}^{N-1} \tilde{X}_k e^{j2\pi k \Delta f t} \right] . e^{-j\omega_0 t} \qquad (5.6)$$

Where, ω_0 is the optical carrier frequency, A_0 is the optical carrier amplitude, N is the total number of subcarriers, Δf is the frequency spacing between OFDM subcarriers and $\tilde{X}_k$ represents the QPSK data symbol. Due to the photodetector square-law detection, the photocurrent is proportional to the received optical power.

$$\tilde{\imath}(t) \propto |A_0|^2 \left| 1 + \sum_{k=0}^{N-1} \tilde{X}_k e^{j2\pi k \Delta f t} \right|^2 \qquad (5.7)$$

Squaring of the received optical field leads to mixing of optical carrier and OFDM subcarriers (desired) and mixing among subcarriers (SSBI). This crosstalk spreads over the complete RF

bandwidth and hence contaminates the received signal. Mixing among subcarriers can be avoided by simply encoding the OFDM data onto and *exponential envelope* expressed as,

$$\tilde{x}(t) = A_0 \exp\left[1 + \sum_{k=0}^{N-1} \tilde{X}_k e^{j2\pi k\Delta f t}\right] . e^{-j\omega_0 t} \qquad (5.8)$$

When the above described optical field is detected by a photo-detector the photocurrent will be,

$$\tilde{\imath}(t) \propto |A_0|^2 \exp\left\{2 \sum_{k=0}^{N-1} \tilde{X}_k e^{j2\pi k\Delta f t}\right\} \qquad (5.9)$$

It can be seen in Equation 5.9 that there is no nonlinear mixing among subcarriers and SSBI crosstalk is avoided. Schuster et al. in [67] also have shown that C-SSB modulation scheme suffers from poor sensitivity (about 6 dB worse than Offset-SSB) and poor tolerance to chromatic dispersion.

The primary focus of our work is to understand and compensate for second-order intermodulation SSBI impairment in a controlled nonlinear medium. A semiconductor optical amplifier (SOA) is used to give a nonlinear transfer function, as previously shown in Fig. 4.3. Next section lists out details of our experiment followed by discussion of results.

5.4 Experimental Setup

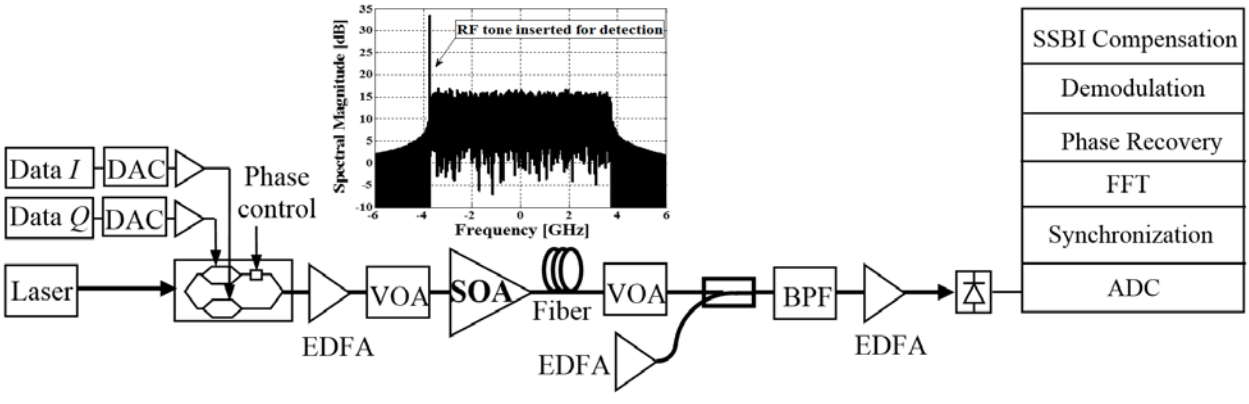

Figure 5.5: Experimental setup (includes inset showing the transmitted spectrum).

The experiment is setup is schematically shown in Figure 5.5. A C-band tunable DFB laser with 10 MHz spectral linewidth is used as the optical source. Virtual single sideband (VSSB) OFDM signal is generated through an *I/Q* modulator which translates the in-phase (*I*) and quadrature (*Q*) data channels into the upper and the lower sidebands of the optical signal and thus the electric bandwidth utilization is doubled. The optical carrier is suppressed by appropriately setting the biasing of the modulator, and an RF tone is inserted at the edge of the negative sideband so that direct detection can be used in the receiver as illustrated in the inset of Figure 5.5. 15 Gb/s data stream in QPSK format is loaded onto 95 subcarriers (out of the total 256 subcarriers) through serial to parallel conversion and IFFT. The data is loaded onto subcarriers 1 through 48 and 210 through 256, and the remaining subcarriers are forced to zero. This results in an optical bandwidth of 7.5 GHz. The RF tone is inserted onto the 209^{th} subcarrier (at −3.75 GHz). The *I* and *Q* components that are fed into a commercial CIENA optical transceiver card [69], are the real and imaginary parts of digitally generated VSSB−OFDM signal. This card is equipped with two DACs with 21.418 GSa/s sampling rate at 6-bits resolution. An EDFA post amplifier is used after the modulator to provide adequate optical power which allows us to explore linear and nonlinear operation regions of an SOA after a variable attenuator (VOA). The SOA used in the experiment is INPHENIX IPSAD 1501 with a small signal gain of 15.4 dB at 200mA driving current. ASE noise generated from an EDFA is loaded into the optical signal through a 3−dB coupler which allows the variation of OSNR at the receiver. An optical band-pass filter (BPF) with 1 nm bandwidth is used to filter out the wide-band ASE noise. The signal optical power at the photodetector is maintained at 0 dBm throughout the experiment. The photocurrent is recorded using a 50 GSa/s digital oscilloscope and signal processing algorithms are implemented offline using MATLAB programming.

5.5 SSBI Compensation Technique

In the direct detection process, the photodiode in the receiver performs squaring operation on the incident optical field. Useful data signals are generated from the mixing between the carrier and subcarriers. At the same time, inter-channel crosstalk is also generated due to the intermixing among subcarriers, known as SSBI. Compensation of SSBI in digital domain is a promising technique to ensure the quality of data transmission. Fig. 5.6(A) illustrates the iterative procedure of SSBI compensation, which relies on the reconstruction of interference waveform and subtracting it from the originally received signal. This process can be repeated multiple times to minimize the effect of SSBI, but the effectiveness diminishes as the number of iteration increases.

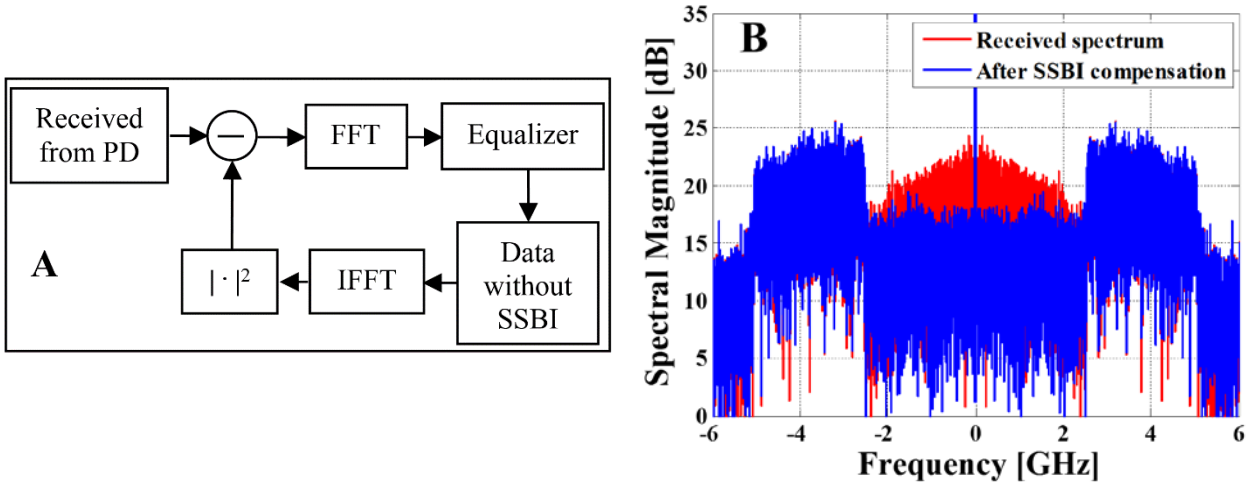

Figure 5.6: Steps involved in SSBI compensation technique (A), comparison of recevied spectrum before and after SSBI compensation (B).

For the purpose of demonstrating the operation principle of SSBI cancellation, we have constructed a conventional band off-set modulation spectrum as shown in Fig. 5.6(B). In this spectrum, the total optical bandwidth is 10 GHz, but a 2.5 GHz guard band is reserved on each side of the optical carrier to elaborate the effect of SSBI in this region. Upon direct detection,

SSBI creates significant crosstalk components inside the guard band (DC to 2.5 GHz) shown as red spectrum in Fig. 5.6(B). The created SSBI has a signature triangular spectral shape originated from the convolution process of signal-signal interference, and thus the strongest impact of SSBI crosstalk is on the OFDM subcarriers closest to optical carrier. The SSBI crosstalk can be significantly reduced through digital compensation based on the procedure shown in Fig. 5.6(A). The electric spectrum after a single iteration of SSBI correction is also shown in Fig. 5.6(B) (blue line), which clearly demonstrates significant reduction of SSBI crosstalk compensation inside the guard band.

5.6 Efficiency of SSBI compensation in a nonlinear system

Although SSBI compensation has been previously demonstrated in directly detected optical systems operating in the linear regime, its effectiveness has not been investigated when the system is significantly nonlinear. In order to quantitatively evaluate the impact of SSBI on the system performance, we use Error vector magnitude (EVM) as the performance metric in our experiments. EVM has shown to be a reliable metric for high level modulated optical signals including linear and nonlinear impairments [49]. An important system parameter determining the effect of SSBI is the carrier-to-signal power ratio (CSPR). A high CSPR results in a low SSBI because the mixing between the carrier and the signal subcarriers is much stronger than the mixing among subcarriers. But an increased CSPR would result in a degradation of the required OSNR in the receiver because a significant portion of the optical power is in the optical carrier and the signal subcarriers are relatively weak. Three different values of CSPR, 2dB, 6dB and 10dB, are used in our experiment.

To study the impact of nonlinearities in the system introduced by the SOA, we consider three different signal optical power levels, −30dBm, −20dBm, and −10dBm, at the input of the SOA. At the injection current of 200mA, the small signal gain of the SOA is 15.4dB, and the 3dB input saturation power is approximately −15dBm.

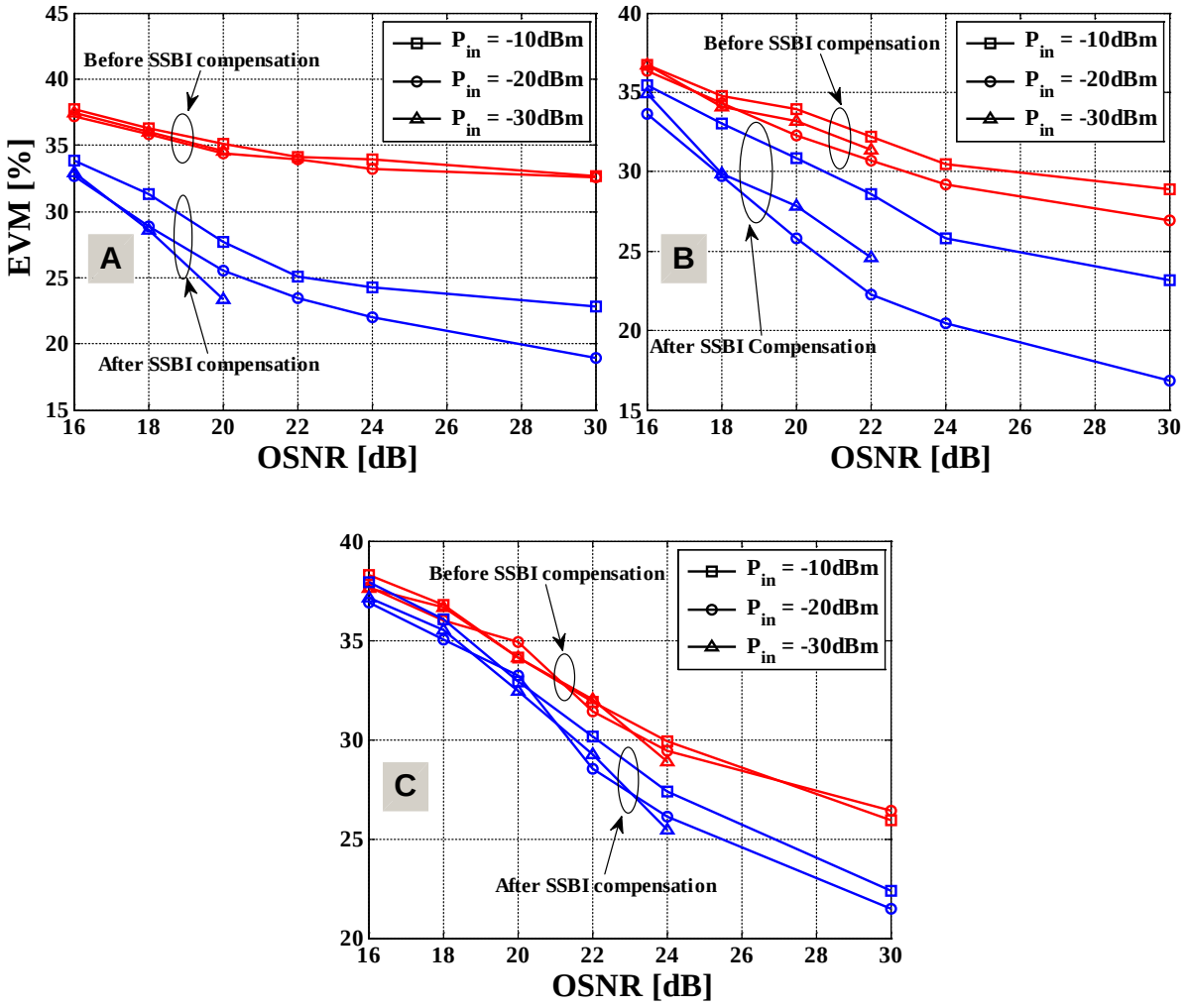

Figure 5.7: EVM as a function of OSNR for various SOA input launch power values. CSPR = 2 dB (A), CSPR = 6 dB (B), and CSPR = 10 dB (C).

In Fig. 5.7, we experimentally determine EVM as a function of optical signal-to-noise ratio (OSNR). The OSNR values were measured by an optical spectrum analyzer (OSA) with 0.1nm spectral resolution. For each value of CSPR, we evaluate system performance in linear as well as nonlinear regime of the SOA, before and after SSBI compensation. Without SSBI compensation, system performance improves with the increase of OSNR, but is relatively independent of the SOA input power levels P_{in} (red lines). However, after SSBI compensation is applied, the reduction in EVM strongly depends on the values of both CSPR and P_{in}. Performance degradation due to SSBI is severe at low CSPR of 2 dB, and becomes less severe as CSPR increases to 6dB, and finally to 10dB. We observe that EVM can be improved significantly (about 14%; for 30dB OSNR) through SSBI compensation for low CSPR case. The corresponding improvement in EVM diminishes to 10% for CSPR = 6 dB, and about 5% for CSPR = 10 dB. Hence, we first conclude that SSBI compensation is most effective when the degradation is mostly due to SSBI because of the low CSPR.

We then evaluate performance of this technique in the nonlinear region (P_{in}=−10 dBm). We observe, besides the first drawn conclusion, that the SSBI compensation technique is not as effective as it was in the linear region. For example, for the same OSNR value of 30 dB, the EVM improvement goes down to 10%, 6%, and 3.5% for CSPR values of 2, 6, and 10 dB, respectively. Therefore, this technique cannot work as a standalone compensation method in the presence of nonlinear impairments. Hence, a more effective technique is needed to compensate for both SSBI and SOA impairments and will be part of our future work.

5.7 Conclusion

We have described SSBI impairment in direct detection systems and classified several prposed solutions. We experimentally evaluated the performance of SSBI compensation technique proposed by Peng et al. in a nonlinear system setup. Our results show that this compensation technique is able to reduce inter-subcarrier mixing when a nonlinear device, such as an SOA operates in the linear region. However, when the SOA is operating in the nonlinear region, SSBI compensation is not able to fully remove mixing at the same CSPR level. A better technique that integrates current SSBI reduction technique with SOA transfer function inversion will be necessary to mitigate interference in such systems.

Chapter 6

Conclusion and future work

Multicarrier optical transmission offers a wide array of benefits and promises to shape future optical telecommunication research and development. However, a multicarrier signaling scheme may lead to inter-subcarrier mixing in certain configurations, such as in (1) radio-over-fiber systems while down converting RF signal to baseband in the customer unit, and (2) direct detection systems where nonlinearity comes from the square-law detection receiver. Nonlinear mixing can also be produced by other optical system element, such as a SOA, which further complicates the mechanism, and increases the level of difficulty for compensation.

In this dissertation, the goal is to understand SSBI impairment in various optical system configurations and propose compensation techniques, in the presence or absence of different nonlinear effects. Our research findings can be summarized as follows;

1. Carrier extraction and reuse (CER) technique proposed for RoF systems is able to significantly reduce SSBI compared to RF self-homodyne technique. CER is able to make overall RoF system design simple and cost effective. The RF carrier for the uplink path need not be additionally generated, as the extracted carrier from the downlink path is reused as the carrier for uplink data.
2. In the case of coherent detection systems, we show that Nyquist sinc-pulse transmission was less susceptible to nonlinear degradation compared to CO-OFDM at the same spectral confinement condition and same bandwidth efficiency. We also experimentally demonstrated that nonlinear region benefitted more from clipping (to reduce PAPR) than the linear region.

3. For multi-carrier optical systems with direct detection and using SOA for optical amplification, we have shown that SSBI contamination can be removed from the useful data carrying signal to a large extent when the optical system operates in the linear region, especially when the carrier-to-signal power ratio is low. However, similar SSBI mitigation in the nonlinear region could not be achieved due to the fast carrier dynamics of the SOA.

There are many research opportunities looking ahead in this area of optical telecommunications.

1. For the RoF systems, the frequency stabilization of the two lasers for optical heterodyne mixing and its effect on the system performance can be further studied. Also, our experimental setup uses the same carrier frequency for both downlink and uplink paths, which might be a significant problem if spatial and time diversity is not used. A carrier frequency adjustment methodology can be developed for a functional bi-directional link without the need of time/spatial diversity.
2. An iterative SSBI compensation technique that works for both linear and nonlinear system configuration needs to be investigated for direct detection systems.
3. Development of real-time optical receivers will allow for more accurate performance monitoring. Field programmable gate array (FPGA) based optical signal generation and reception will allow researchers to better understand and establish system limitations with respect to performance, system complexity, and energy conservation.

References

[1] R. Hui and M. O'Sullivan, *Fiber optic measurement techniques*: Academic Press, 2009.

[2] N. Massa, "Fiber optic telecommunication," *Fundamentals of Photonics. University of Conneticut*, 2000.

[3] M. A. Bourouha, M. Bataineh, and M. Guizani, "Advances in optical switching and networking: past, present, and future," in *SoutheastCon, 2002. Proceedings IEEE*, 2002, pp. 405-413.

[4] N. Corp., "World record one petabit per second fiber transmission over 50 km: equivalent to sending 5,000 HDTV videos per second over a single fiber," September 2012.

[5] W. Shieh and C. Athaudage, "Coherent optical orthogonal frequency division multiplexing," *Electronics Letters*, vol. 42, pp. 587-589, 2006.

[6] A. J. Lowery and J. Armstrong, "Orthogonal-frequency-division multiplexing for dispersion compensation of long-haul optical systems," *Opt. Express*, vol. 14, pp. 2079-2084, 2006.

[7] I. B. Djordjevic and B. Vasic, "Orthogonal frequency division multiplexing for high-speed optical transmission," *Opt. Express*, vol. 14, pp. 3767-3775, 2006.

[8] D. Falconer, S. L. Ariyavisitakul, A. Benyamin-Seeyar, and B. Eidson, "Frequency domain equalization for single-carrier broadband wireless systems," *Communications Magazine, IEEE*, vol. 40, pp. 58-66, 2002.

[9] Z. Wang, X. Ma, and G. B. Giannakis, "OFDM or single-carrier block transmissions?," *Communications, IEEE Transactions on*, vol. 52, pp. 380-394, 2004.

[10] D. Qian, J. Hu, J. Yu, P. N. Ji, L. Xu, T. Wang, *et al.*, "Experimental demonstration of a novel OFDM-A based 10Gb/s PON architecture," *ECOC 2007*, 2007.

[11] W. Shieh, Q. Yang, and Y. Ma, "107 Gb/s coherent optical OFDM transmission over 1000-km SSMF fiber using orthogonal band multiplexing," *Optics express,* vol. 16, pp. 6378-6386, 2008.

[12] S. L. Jansen, I. Morita, T. C. Schenk, and H. Tanaka, "121.9-Gb/s PDM-OFDM transmission with 2-b/s/Hz spectral efficiency over 1000 km of SSMF," *Journal of Lightwave Technology,* vol. 27, pp. 177-188, 2009.

[13] J. Yu, X. Zhou, M.-F. Huang, Y. Shao, D. Qian, T. Wang, *et al.*, "Tb/s (161× 114 Gb/s) PolMux-RZ-8PSK transmission over 662 km of ultra-low loss fiber using C-band EDFA amplification and digital coherent detection," in *Proceedings of European Conference on Optical Communication (ECOC), Th*.

[14] B. Spinnler, F. Hauske, and M. Kuschnerov, "Adaptive equalizer complexity in coherent optical receivers," in *2008 34th European Conference on Optical Communication*, 2008.

[15] R. Hui, W. Huang, Y. Zhang, M. Hameed, M. Razo, M. Tacca, *et al.*, "Digital subcarrier optical networks and cross-connects," *Journal of High Speed Networks,* vol. 19, pp. 55-69, 2013.

[16] J. Zhao and A. D. Ellis, "A novel optical fast OFDM with reduced channel spacing equal to half of the symbol rate per carrier," in *Optical Fiber Communication Conference*, 2010.

[17] R. Schmogrow, S. Wolf, B. Baeuerle, D. Hillerkuss, B. Nebendahl, C. Koos, *et al.*, "Nyquist frequency division multiplexing for optical communications," in *CLEO: Science and Innovations*, 2012.

[18] A. Barbieri, D. Fertonani, and G. Colavolpe, "Time-frequency packing for linear modulations: spectral efficiency and practical detection schemes," *Communications, IEEE Transactions on,* vol. 57, pp. 2951-2959, 2009.

[19] G. Bosco, A. Carena, V. Curri, P. Poggiolini, and F. Forghieri, "Performance limits of Nyquist-WDM and CO-OFDM in high-speed PM-QPSK systems," *Photonics Technology Letters, IEEE,* vol. 22, pp. 1129-1131, 2010.

[20] W. Shieh, H. Bao, and Y. Tang, "Coherent optical OFDM: theory and design," *Opt. Express,* vol. 16, pp. 841-859, 2008.

[21] W. Shieh and I. Djordjevic, *OFDM for optical communications*: Academic Press, 2009.

[22] Y. Zhang, "SPECTRALLY EFFICIENT MULTICARRIER SYSTEMS FOR FIBER-OPTIC TRANSMISSION," 2012.

[23] G. Bosco, V. Curri, A. Carena, P. Poggiolini, and F. Forghieri, "On the performance of Nyquist-WDM terabit superchannels based on PM-BPSK, PM-QPSK, PM-8QAM or PM-16QAM subcarriers," *Journal of Lightwave Technology,* vol. 29, pp. 53-61, 2011.

[24] M. A. Hameed, M. O'Sullivan, and R. Hui, "Impact of SOA-Induced Nonlinear Impairments in CO-OFDM and Nyquist Sinc-Pulse Transmission," in *Asia Communications and Photonics Conference*, 2013, p. AF3E. 4.

[25] M. Hameed and R. Hui, "Simplified RF carrier extraction and reuse in OFDM Radio-Over-Fiber systems," *IEEE Photonics Technology Letters,* vol. 26, pp. 1734-1737, 2014.

[26] Y. Benlachtar, G. Gavioli, V. Mikhailov, and R. I. Killey, "Experimental investigation of SPM in long-haul direct-detection OFDM systems," *Optics express,* vol. 16, pp. 15477-15482, 2008.

[27] M. Shtaif, "Analytical description of cross-phase modulation in dispersive optical fibers," *Optics letters*, vol. 23, pp. 1191-1193, 1998.

[28] Z. Cao, J. Yu, W. Wang, L. Chen, and Z. Dong, "Direct-detection optical OFDM transmission system without frequency guard band," *Photonics Technology Letters, IEEE*, vol. 22, pp. 736-738, 2010.

[29] W.-R. Peng, B. Zhang, K.-M. Feng, X. Wu, A. E. Willner, and S. Chi, "Spectrally efficient direct-detected OFDM transmission incorporating a tunable frequency gap and an iterative detection techniques," *Lightwave Technology, Journal of*, vol. 27, pp. 5723-5735, 2009.

[30] A. Li, D. Che, X. Chen, Q. Hu, Y. Wang, and W. Shieh, "61 Gbits/s direct-detection optical OFDM based on blockwise signal phase switching with signal-to-signal beat noise cancellation," *Optics letters*, vol. 38, pp. 2614-2616, 2013.

[31] J. Ma, "Simple signal-to-signal beat interference cancellation receiver based on balanced detection for a single-sideband optical OFDM signal with a reduced guard band," *Optics letters*, vol. 38, pp. 4335-4338, 2013.

[32] S. A. Nezamalhosseini, L. R. Chen, Q. Zhuge, M. Malekiha, F. Marvasti, and D. V. Plant, "A Novel Receiver for Spectrally Efficient Direct Detection Optical OFDM," in *Photonics Conference (IPC), 2013 IEEE*, 2013, pp. 539-540.

[33] B. J. Schmidt, Z. Zan, L. B. Du, and A. J. Lowery, "100 Gbit/s Transimssion Using Single-Band Direct-Detection Optical OFDM," in *Optical Fiber Communication Conference*, 2009, p. PDPC3.

[34] D. J. Mestdagh, P. Spruyt, and B. Biran, "Analysis of clipping effect in DMT-based ADSL systems," in *Communications, 1994. ICC'94, SUPERCOMM/ICC'94, Conference*

Record,'Serving Humanity Through Communications.'IEEE International Conference on, 1994, pp. 293-300.

[35] M. Bernhard, D. Rörich, T. Handte, and J. Speidel, "Analytical and numerical studies of quantization effects in coherent optical OFDM transmission with 100Gbit/s and beyond," *ITG-Fachbericht-Photonische Netze*, 2012.

[36] R. Schmogrow, M. Winter, M. Meyer, D. Hillerkuss, S. Wolf, B. Baeuerle, *et al.*, "Real-time Nyquist pulse generation beyond 100 Gbit/s and its relation to OFDM," *Optics Express*, vol. 20, pp. 317-337, 2012.

[37] J. G. Proakis, "Digital communications. 1995," *McGraw-Hill, New York*.

[38] J. Wells, "Faster than fiber: The future of multi-G/s wireless," *Microwave Magazine, IEEE*, vol. 10, pp. 104-112, 2009.

[39] R.-P. Braun, G. Grosskopf, D. Rohde, and F. Schmidt, "Low-phase-noise millimeter-wave generation at 64 GHz and data transmission using optical sideband injection locking," *Photonics Technology Letters, IEEE*, vol. 10, pp. 728-730, 1998.

[40] L. Johansson and A. Seeds, "Generation and transmission of millimeter-wave data-modulated optical signals using an optical injection phase-lock loop," *Lightwave Technology, Journal of*, vol. 21, pp. 511-520, 2003.

[41] A. Islam, M. Bakaul, and A. Nirmalathas, "Multi-level Modulations for Gigabit Access in a Simple Millimeter-Wave Radio-over-Fiber Link," *Photonics Technology Letters, IEEE* vol. 24, pp. 1860-1863, October, 2012 2012.

[42] J. O'Reilly and P. Lane, "Remote delivery of video services using mm-waves and optics," *Lightwave Technology, Journal of*, vol. 12, pp. 369-375, 1994.

[43] A. Islam, M. Bakaul, A. Nirmalathas, and G. E. Town, "Simplification of millimeter-wave radio-over-fiber system employing heterodyning of uncorrelated optical carriers and self-homodyning of RF signal at the receiver," *Optics express,* vol. 20, pp. 5707-5724, 2012.

[44] C.-T. Lin, J. Chen, P.-T. Shih, W.-J. Jiang, and S. Chi, "Ultra-high data-rate 60 GHz radio-over-fiber systems employing optical frequency multiplication and OFDM formats," *Lightwave Technology, Journal of,* vol. 28, pp. 2296-2306, 2010.

[45] T. Kuri, H. Toda, J. J. V. Olmos, and K.-i. Kitayama, "Reconfigurable dense wavelength-division-multiplexing millimeter-waveband radio-over-fiber access system technologies," *Lightwave Technology, Journal of,* vol. 28, pp. 2247-2257, 2010.

[46] J. D. Gaudette, D. J. Krause, J. C. Cartledge, and K. Roberts, "Offset sideband modulation at 2.5 GSym/s," in *Optical Fiber Communication Conference*, 2007.

[47] S. J. Savory, "Digital filters for coherent optical receivers," *Optics Express*, vol. 16, pp. 804-817, 2008.

[48] A. Goldsmith, *Wireless communications*: Cambridge university press, 2005.

[49] R. Schmogrow, B. Nebendahl, M. Winter, A. Josten, D. Hillerkuss, S. Koenig, *et al.*, "Error vector magnitude as a performance measure for advanced modulation formats," *Photonics Technology Letters, IEEE,* vol. 24, pp. 61-63, 2012.

[50] P. Morel, P. Chanclou, R. Brenot, T. Motaweh, M. Guégan, and A. Sharaiha, "Experimental demonstration of SOAs optical bandwidth widening based on selective filtering," in *Semiconductor Laser Conference (ISLC), 2010 22nd IEEE International*, 2010, pp. 107-108.

[51] W. Shieh, "High spectral efficiency coherent optical OFDM for 1 Tb/s ethernet transport," in *Optical Fiber Communication Conference*, 2009, p. OWW1.

[52] M. Mayrock and H. Haunstein, "Performance monitoring in optical OFDM systems," in *Optical Fiber Communication Conference*, 2009, p. OWM3.

[53] W. Shieh, R. S. Tucker, W. Chen, X. Yi, and G. Pendock, "Optical performance monitoring in coherent optical OFDM systems," *Optics express,* vol. 15, pp. 350-356, 2007.

[54] J. Baliga, K. Hinton, and R. S. Tucker, *Energy consumption of the Internet*: University of Melbourne, Department of Electrical and Electronic Engineering, 2011.

[55] A. Vukovic, "Network power density challenges," *ASHRAE journal,* vol. 47, p. 55, 2005.

[56] M. Gupta and S. Singh, "Greening of the Internet," in *Proceedings of the 2003 conference on Applications, technologies, architectures, and protocols for computer communications*, 2003, pp. 19-26.

[57] H. Khaleghi, A. Sharaiha, T. Rampone, P. Morel, and M. Guegan, "Semiconductor Optical Amplifiers in Coherent Optical-OFDM Systems," *Photonics Technology Letters, IEEE,* vol. 24, pp. 560-562, 2012.

[58] R. Bonk, G. Huber, T. Vallaitis, R. Schmogrow, D. Hillerkuss, C. Koos, *et al.*, "Impact of alfa-factor on SOA dynamic range for 20 GBd BPSK, QPSK and 16-QAM signals," in *Optical Fiber Communication Conference*, 2011.

[59] Y. Zhang, M. O'Sullivan, and R. Hui, "Digital subcarrier multiplexing for flexible spectral allocation in optical transport network," *Opt. Express19 (22),* pp. 21880-21889, 2011.

[60] B. Kozicki, H. Takara, Y. Tsukishima, T. Yoshimatsu, K. Yonenaga, and M. Jinno, "Experimental demonstration of spectrum-sliced elastic optical path network (SLICE)," *Optics express,* vol. 18, pp. 22105-22118, 2010.

[61] J. Xiao, J. Yu, X. Li, Q. Tang, H. Chen, F. Li, *et al.*, "Hadamard Transform Combined With Companding Transform Technique for PAPR Reduction in an Optical Direct-Detection OFDM System," *Journal of Optical Communications and Networking,* vol. 4, pp. 709-714, 2012.

[62] X. Li, L. Tao, J. Zhang, Y. Wang, Y. Fang, J. Zhu, *et al.*, "Companding transform for PAPR reduction in coherent optical OFDM system," in *Wireless and Optical Communications Conference (WOCC), 2012 21st Annual*, 2012, pp. 46-47.

[63] W. Zou, J. Yu, J. Xiao, and L. Chen, "Direct-detection Optical Orthogonal Frequency Division Multiplexing System with New Training Sequence," *Frequenz,* vol. 66, pp. 27-32, 2012.

[64] W.-R. Peng, X. Wu, K.-M. Feng, V. R. Arbab, B. Shamee, J.-Y. Yang, *et al.*, "Spectrally efficient direct-detected OFDM transmission employing an iterative estimation and cancellation technique," *Optics express,* vol. 17, pp. 9099-9111, 2009.

[65] D. F. Hewitt, "Orthogonal frequency division multiplexing using baseband optical single sideband for simpler adaptive dispersion compensation," in *Proc. OFC/NFOEC,* 2007, pp. 25-29.

[66] W.-R. Peng, X. Wu, V. R. Arbab, K.-M. Feng, B. Shamee, L. C. Christen, *et al.*, "Theoretical and experimental investigations of direct-detected RF-tone-assisted optical OFDM systems," *Journal of Lightwave Technology,* vol. 27, pp. 1332-1339, 2009.

[67] M. Schuster, S. Randel, C. A. Bunge, S. C. J. Lee, F. Breyer, B. Spinnler, *et al.*, "Spectrally efficient compatible single-sideband modulation for OFDM transmission with direct detection," *IEEE Photonics Technology Letters*, vol. 20, p. 670, 2008.

[68] Y. Zhang, M. O'Sullivan, and R. Hui, "Theoretical and experimental investigation of compatible SSB modulation for single channel long-distance optical OFDM transmission," *Opt. Express18 (16)*, pp. 16751-16764, 2010.

[69] J. McNicol, M. O'Sullivan, K. Roberts, A. Comeau, D. McGhan, and L. Strawczynski, "Electronic domain compensation of optical dispersion," in *Optical Fiber Communication Conference*, 2005, p. OThJ3.

Appendix

Phase sensitivity of Carrier extraction and reuse technique

Let the electric fields of two lasers used in figure 3.3 be,

$$E_1 e^{i(2\pi f_1 t+\emptyset_1)}$$

$$E_2 e^{i(2\pi f_2 t+\emptyset_2)}$$

The first laser is modulated using a sinusoid $m\cos 2\pi f_m t$ and the second laser is unmodulated and is used to generate RF carrier by optical heterodyning at the PD.

Electric fields of modulated and unmodulated optical carriers are:

$$A_1(t) = e^{i(2\pi f_1 t+\emptyset_1)} + \frac{m}{2}[e^{i(2\pi f_1 t+\emptyset_1+2\pi f_m t)} + e^{i(2\pi f_1 t+\emptyset_1-2\pi f_m t)}] \quad (1)$$

$$A_2(t) = e^{i(2\pi f_2 t+\emptyset_2)} \quad (2)$$

After transmission over the SMF these equation can be written as;

$$A_{f1}(t) = e^{i(2\pi f_1 t+\emptyset_1+\theta_0)} + \frac{m}{2}[e^{i\{2\pi(f_1+f_m)t+\emptyset_1+\theta_1\}} + e^{i\{2\pi(f_1-f_m)t+\emptyset_1+\theta_2\}}] \quad (3)$$

$$A_{f2}(t) = e^{i(2\pi f_2 t+\emptyset_2+\theta_3)} \quad (4)$$

The complex conjugates of (3) and (4) can be written as;

$$A^*_{f1}(t) = e^{-i(2\pi f_1 t+\emptyset_1+\theta_0)} + \frac{m}{2}[e^{-i\{2\pi(f_1+f_m)t+\emptyset_1+\theta_1\}} + e^{-i\{2\pi(f_1-f_m)t+\emptyset_1+\theta_2\}}] \quad (5)$$

$$A^*_{f2}(t) = e^{-i(2\pi f_2 t+\emptyset_2+\theta_3)} \quad (6)$$

Optical heterodyning at the photodetector generates a RF signal given by,

$$i_p(t) = R \times \left[\left(A_{f1}(t) + A_{f2}(t)\right) \times \left(A^*_{f1}(t) + A^*_{f2}(t)\right)\right]$$

$$= R \times \left[1 + \frac{m}{2} e^{-i(2\pi f_m t + \theta_1 - \theta_0)} + \frac{m}{2} e^{i(2\pi f_m t + \theta_0 - \theta_2)} + e^{i(2\pi(f_1 - f_2)t + \emptyset_1 - \emptyset_2 + \theta_0 - \theta_3)}\right.$$

$$+ \frac{m}{2} e^{i(2\pi f_m t + \theta_1 - \theta_0)} + \frac{m^2}{4} + \frac{m^2}{4} e^{i(2\pi 2 f_m t + \theta_1 - \theta_2)}$$

$$+ \frac{m}{2} e^{i(2\pi(f_1 - f_2 + f_m)t + \emptyset_1 - \emptyset_2 + \theta_1 - \theta_3)} + \frac{m}{2} e^{-i(2\pi f_m t + \theta_0 - \theta_2)} + \frac{m^2}{4} e^{-i(2\pi 2 f_m t + \theta_1 - \theta_2)}$$

$$+ \frac{m^2}{4} + \frac{m}{2} e^{i(2\pi(f_1 - f_2 - f_m)t + \emptyset_1 - \emptyset_2 + \theta_2 - \theta_3)} + e^{-i(2\pi(f_1 - f_2)t + \emptyset_1 - \emptyset_2 + \theta_0 - \theta_3)}$$

$$\left. + \frac{m}{2} e^{-i(2\pi(f_1 - f_2 + f_m)t + \emptyset_1 - \emptyset_2 + \theta_1 - \theta_3)} + \frac{m}{2} e^{-i(2\pi(f_1 - f_2 - f_m)t + \emptyset_1 - \emptyset_2 + \theta_2 - \theta_3)} + 1\right]$$

$$= R \times \left[2 + m\cos(2\pi f_m t + \theta_1 - \theta_0) + m\cos(2\pi f_m t + \theta_0 - \theta_2)\right.$$

$$+ 2\cos(2\pi(f_1 - f_2)t + \emptyset_1 - \emptyset_2 + \theta_0 - \theta_3) + \frac{m^2}{2} + \frac{m^2}{2}\cos(2\pi 2 f_m t + \theta_1 - \theta_2)$$

$$+ m\cos(2\pi(f_1 - f_2 + f_m)t + \emptyset_1 - \emptyset_2 + \theta_1 - \theta_3)$$

$$\left. + m\cos(2\pi(f_1 - f_2 - f_m)t + \emptyset_1 - \emptyset_2 + \theta_2 - \theta_3)\right] \qquad (7)$$

The extracted RF carrier at (f_1-f_2) is given by (half power because of splitter),

$$C(t) = R\cos\{2\pi(f_1 - f_2)t + \emptyset_1 - \emptyset_2 + \theta_0 - \theta_3\} \qquad (8)$$

RF self-mixing process results in (Eq. 7 multiplied by Eq. 8)

$$\frac{i_p(t)}{2} \times C(t) = 2R^2 \cos\{2\pi(f_1 - f_2)t + \emptyset_1 - \emptyset_2 + \theta_0 - \theta_3\}$$

$$+ \frac{mR^2}{2}\cos\{2\pi(f_1 - f_2 + f_m)t + \emptyset_1 - \emptyset_2 + \theta_1 - \theta_3\}$$

$$+ \frac{mR^2}{2}\cos\{2\pi(f_1 - f_2 - f_m)t + \emptyset_1 - \emptyset_2 + 2\theta_0 - \theta_1 - \theta_3\}$$

$$+ \frac{mR^2}{2}\cos\{2\pi(f_1 - f_2 + f_m)t + \emptyset_1 - \emptyset_2 + 2\theta_0 - \theta_2 - \theta_3\}$$

$$+ \frac{mR^2}{2}\cos\{2\pi(f_1 - f_2 - f_m)t + \emptyset_1 - \emptyset_2 + \theta_2 - \theta_3\}$$

$$+ R^2 \cos\{2[2\pi(f_1 - f_2)t + \emptyset_1 - \emptyset_2 + \theta_0 - \theta_3]\} + R^2$$

$$+ \frac{m^2R^2}{2}\cos\{2\pi(f_1 - f_2)t + \emptyset_1 - \emptyset_2 + \theta_0 - \theta_3\}$$

$$+ m^2R^2 \cos\{2\pi(f_1 - f_2 + 2f_m)t + \emptyset_1 - \emptyset_2 + \theta_1 - \theta_2\}$$

$$+ m^2R^2 \cos\{2\pi(f_1 - f_2 - 2f_m)t + \emptyset_1 - \emptyset_2 + \theta_0 - \theta_3 - \theta_1 + \theta_2\}$$

$$+ \frac{mR^2}{2}\cos\{2\pi(f_m)t + \theta_1 - \theta_0\}$$

$$+ \frac{mR^2}{2}\cos\{2\pi(2f_1 - 2f_2 + f_m)t + 2\emptyset_1 - 2\emptyset_2 + \theta_0 + \theta_1 - 2\theta_3\}$$

$$+ \frac{mR^2}{2}\cos\{2\pi(f_m)t + \theta_0 - \theta_2\}$$

$$+ \frac{mR^2}{2}\cos\{2\pi(2f_1 - 2f_2 - f_m)t + 2\emptyset_1 - 2\emptyset_2 + \theta_0 + \theta_2 - 2\theta_3\}$$

If we assume fiber dispersion is negligible (i.e.≈ 0) and use a filter to extract the baseband signal at f_m, the above equation can be written as:

$$\text{received signal} = mR^2 \cos\{2\pi(f_m)t\}$$